



# A National Scale Hybrid Model for Enhanced Streamflow Estimation - Consolidating a Physically Based Hydrological Model with Long Short-term Memory Networks

Jun Liu, Julian Koch, Simon Stisen, Lars Troldborg, Raphael J. M. Schneider

5 Department of hydrology, Geological Survey of Denmark and Greenland, Copenhagen, 1350, Denmark

*Correspondence to:* Jun Liu (juliu@geus.dk)

**Abstract.** Accurate streamflow estimation is essential for effective water resources management and adapting to extreme events in the face of changing climate conditions. Hydrological models have been the conventional approach for streamflow inter/extrapolation in time and space for the past decades. However, their large-scale applications have encountered challenges, including issues related to efficiency, complex parameterization, and constrained performance. Deep learning methods, such as Long Short-Term Memory networks (LSTM), have emerged as a promising and efficient approach for large-scale streamflow estimation. In this study, we conducted a series of experiments to identify optimal hybrid modelling schemes to consolidate physically based models with LSTM aimed at enhancing streamflow estimation in Denmark.

The results showed that the hybrid modelling schemes outperformed the Danish Water Resources Model (DKM) in both gauged and ungauged basins. While the standalone LSTM rainfall-runoff model outperformed DKM in many basins, it faced challenges when predicting streamflow in groundwater-dependent catchments. A serial hybrid modelling scheme (LSTM-q), which used DKM outputs and climate forcings as dynamic inputs for LSTM training, demonstrated higher performance. LSTM-q improved the median Nash-Sutcliffe Efficiency (NSE) by 0.18 in gauged basins and 0.11 in ungauged basins compared to DKM. Similar accuracy improvements were achieved with alternative hybrid schemes, i.e., by predicting the residuals between DKM-simulated streamflow and observations using a LSTM. Moreover, the developed hybrid models enhanced the accuracy of extreme events, which encourages the integration of hybrid models within an operational forecasting framework. This study highlights the advantages of synergizing existing physically based hydrological models with LSTM models, and the proposed hybrid schemes hold the potential to achieve high-quality, large-scale streamflow estimations.

## 1 Introduction

25 Accurate streamflow estimates are essential for sustainable water resource management, prediction of extreme events, energy production, decision making, and the protection of both human populations and natural ecosystems (Devitt et al., 2023; Hoy, 2017; Satoh et al., 2022). Collecting spatiotemporally adequate streamflow data through observations can be challenging. Therefore, various conceptual and process-based hydrological models have been developed and applied for streamflow extra/interpolation in time and space (Beven, 1996, 2020; Devia et al., 2015). These models are based on a priori knowledge



30 and physical principles to simulate critical hydrological processes, e.g., infiltration, evapotranspiration, runoff routing, and groundwater movement, and have been widely and successfully used across domains and scales.

Physically based distributed models (PBMs) stand out among those diverse hydrological models and have been widely used in recent decades due to their sophisticated structures and advanced parameterizations (Devia et al., 2015; Fatichi et al., 2016; Pakoksung and Takagi, 2021; Refsgaard et al., 2022). These features enable PBMs to simulate complex hydrological processes and facilitate detailed analysis at high spatiotemporal resolutions. However, PBMs are susceptible to biases arising from inadequate inputs, suboptimal structural design, or improper parameterization schemes (Herrera et al., 2022; Dembélé et al., 2020; Silvestro et al., 2015; Koch et al., 2016). Therefore, the streamflow performance of PBMs is not always satisfactory for practical applications and may not consistently outperform simpler lumped and conceptual hydrological models. For example, some studies have pointed out that PBMs encounter difficulties in capturing peak flows (Baroni et al., 2019; Kumari et al., 2021; Moges et al., 2021; Sahraei et al., 2020).

The Danish Water Resources Model (DKM) is an example of PBM (Højberg et al., 2009), which is based on the distributed, integrated model code MIKE SHE (DHI, 2020). The DKM has been calibrated against a large dataset of groundwater head observations, and streamflow measurements utilizing dense national monitoring networks (Henriksen et al., 2021; Stisen et al., 2020). Streamflow performance is considered satisfactory, with an average Kling-Gupta Efficiency (KGE) of 0.75, though performance varies both temporally and spatially. Overall, the DKM tends to exhibit better performance in basins with larger drainage areas compared to smaller ones (Henriksen et al., 2021). In recent years, several projects related to hydrological monitoring, national flood warning, and nitrate modelling have emerged that rely on DKM-simulated streamflow time series (Henriksen et al., 2023). Therefore, enhancing the accuracy of DKM simulations using advanced methods, such as deep learning (DL) algorithms, is deemed necessary and will have far reaching implications for a range of applications.

Data-driven techniques are well suited for capturing patterns and relationships within data, without relying on prior assumptions or models (Kawaguchi et al., 2022; Ke et al., 2017; Rätsch, 2004; Wu et al., 2022). The runoff process is intricately connected to climate records and other processes in the water cycle. These relationships can be learned through data-driven methods, such as LSTM (Wi and Steinschneider, 2023; Wang et al., 2023; Kratzert et al., 2018). LSTM is a type of recurrent neural network proficient in handling time series data and has proven to effectively capture the variations and dependencies within sequential data (Hochreiter and Schmidhuber, 1997; Greff et al., 2017). It has found successful applications in hydrology, particularly for estimating streamflow in numerous catchments, with encouraging performance (Arsenault et al., 2023; Hunt et al., 2022; Cheng et al., 2020; Zhang et al., 2022; Hashemi et al., 2022; Lees et al., 2021; Wilbrand et al., 2023; Frame et al., 2021a). Nonetheless, concerns exist regarding DL methods, such as their inherently complex internal structures (Ghorbani and Zou, 2019; Goldstein et al., 2015). While they often yield higher performance, accuracy can decrease when attempting to transfer models from gauged basins to ungauged ones. Therefore, the integration of DL methods with PBMs and the development of hybrid systems have been recognized as a promising approach to robustly enhance streamflow predictions (Slater et al., 2023). In such hybrid modelling schemes, PBMs provide a substantial amount of sequential data containing



consolidated hydrological knowledge within the simulation domain, while deep learning algorithms have the potential to exploit multiple data types and uncover information that may be overlooked or ignored by PBMs.

65 A straightforward approach to develop hybrid models is to set up a serial system that uses the outputs of existing PBMs as inputs for LSTM modelling (Amendola et al., 2020; Slater et al., 2023). This approach offers several benefits. For instance, they are efficient and require fewer modifications to the existing PBMs, which may have undergone decades of development and contain valuable physical knowledge. Attempts have been made in various regions where DL methods were employed to post-process imperfect PBM simulations (Cho and Kim, 2022; Frame et al., 2021b; Konapala et al., 2020; Liu et al., 2022; 70 Shen et al., 2022). While earlier studies have explored different hybrid systems, there remain scientific aspects that warrant further investigation:

1. What are the optimal hybrid schemes for combining PBMs and LSTM in Denmark?

While earlier studies have explored a limited number of alternative hybrid modelling schemes, the full potential of intercomparing different hybrid modelling schemes and a systematic comparison and evaluation of the alternative approaches 75 remains untapped. Frame et al., (2021), Tang et al., (2023), and Liu et al., (2022) evaluated the potential benefit of PBMs outputs and climate forcings as LSTM inputs, with streamflow as the target variable for prediction. Their results indicated a significant improvement in the performance of streamflow estimation by hybrid models compared to benchmark models, i.e., the National Water Model, Global Hydrological Models and WRF-Hydro. Cho and Kim (2022) and Konapala et al., (2020) investigate the performance of a LSTM model, which predicts the residuals between WRF-Hydro simulated discharge and 80 observations. Koch and Schneider (2022) proposed that an LSTM model pretrained with DKM simulated discharge as the target variable, followed by fine-tuning with observed discharge, yielded superior results. These studies offer intriguing approaches to consolidate PBMs with LSTM in hybrid modelling schemes. It is imperative to evaluate these approaches to identify the optimal methods.

2. How can we expand the scope of studies on LSTM models to encompass national scales and groundwater-dependent 85 systems?

To date, research on LSTM models has focused on rainfall-runoff processes in gauged basins, such as the Catchment Attributes and Meteorology for Large-sample Studies (CAMELS-US) dataset (Addor et al., 2017), CAMELS-UK dataset (Coxon et al., 2020), and Global Runoff Data Centre (Tang et al., 2023). Many studies have investigated local basins with limited data coverage (Cho and Kim, 2022; Hunt et al., 2022; Liu et al., 2022). However, there is a notable absence of studies that expand 90 simulations to national scale, i.e., making predictions for all catchments gauged and ungauged and provide a comprehensive map of biases between DL and PBM models. In our study, Denmark, delineated in 2830 catchments, serves as the study area, potentially enriching the geographical scope of this topic.

3. What is the impact of physical processes on LSTM performance in groundwater-dependent areas, and how can we bridge the gap between LSTM and physical knowledge?

95 Connecting LSTM with physical knowledge is an active area of research. Investigating the influence of physical processes on LSTM performance in complex hydrological settings, such as groundwater-dependent flow regimes, is crucial. While previous



studies have explored the effects of snow melting (Frame et al., 2021b; Fuente et al., 2023; Kratzert et al., 2019a; Wang et al., 2022) on LSTM modelling, limited attention has been given to the impacts of groundwater variations on LSTM rainfall-runoff modelling. This gap may be due to the scarcity of observations or the absence of well-established groundwater modelling systems like DKM to support such analyses. Therefore, DKM serves as a valuable testbed for investigating the enhancement of physically informed data-driven models in groundwater-dependent regions.

4. What is the potential of LSTM hybrid models for streamflow estimation in operational frameworks, especially for extreme events?

As the frequency of extreme events is projected to increase in the coming decades, there is growing demand for real-time modelling and forecasting (Curceac et al., 2020; Devitt et al., 2023; Hauswirth et al., 2021). Operational real-time modelling and forecasting frameworks are thus under development with the primary objective of delivering timely warnings, usually based on a short simulation period of hindcasting, nowcasting and forecasting (Nevo et al., 2022). In this context, only few studies have investigated the potential applicability of LSTM hybrid schemes on short simulation periods with a focus of extreme events. Hunt et al. (2022) examined the performance of LSTM models trained to ingest catchment-mean meteorological and hydrological variables from the Global Flood Awareness System (GloFAS)–ERA5 reanalysis and output streamflow at ten hydrological stations in the western US. They utilized the European Centre for Medium-Range Weather Forecasts (ECMWF) Integrated Forecasting System (IFS) to feed the models, predicting streamflow with a lead time of ten days. Their study demonstrated the potential of hybrid LSTM models in the context of operational forecast. The developed LSTM hybrid schemes from this study are expected to support the initiative towards operational modelling in Denmark. Thus, the developed models are specifically assessed during extreme events.

The aim of this study is to test various hybrid systems combining LSTM and DKM and identify optimal LSTM hybrid schemes tailored to streamflow modelling, with applicability in generating continuous streamflow predictions across Denmark with daily timestep.

## 2 Methods and data

This section begins with a description of the LSTM algorithm (Section 2.1), followed by data collection and the introduction of the benchmark model, DKM and LSTM rainfall-runoff model (Section 2.2). Subsequently, Section 2.3 outlines various candidate LSTM hybrid modelling schemes. Details regarding the experiment designs are provided in Section 2.4, and Section 2.5 presents the description of evaluation metrics for assessing model performance.

### 2.1 Long short-term memory networks (LSTM)

LSTM is a type of recurrent neural networks (RNNs) specifically developed to address the shortcomings of traditional RNNs when confronted with sequences featuring long-term dependencies (Hochreiter and Schmidhuber, 1997; Sutskever et al., 2014; Rahmani et al., 2020; Gers et al., 2000; Greff et al., 2017; Kratzert et al., 2018). These networks possess the remarkable ability



to selectively retain or discard information over extended sequences. They achieve this by using specialized memory cells that store and update information as it traverses the networks (Gers et al., 2000). LSTM networks are equipped with multiple hidden unit sizes and incorporate essential information processing instants, namely the input, forget, and output gates. These gates play main roles in regulating the flow of sequential information, enabling the network to determine what information should be preserved and what should be discarded at each time step. While a comprehensive understanding of LSTM networks can be found in numerous studies, readers with a background in hydrology are encouraged to explore the works of Kratzert et al. (2018) for more detailed insights.

## 135 2.2 Dataset and benchmark model

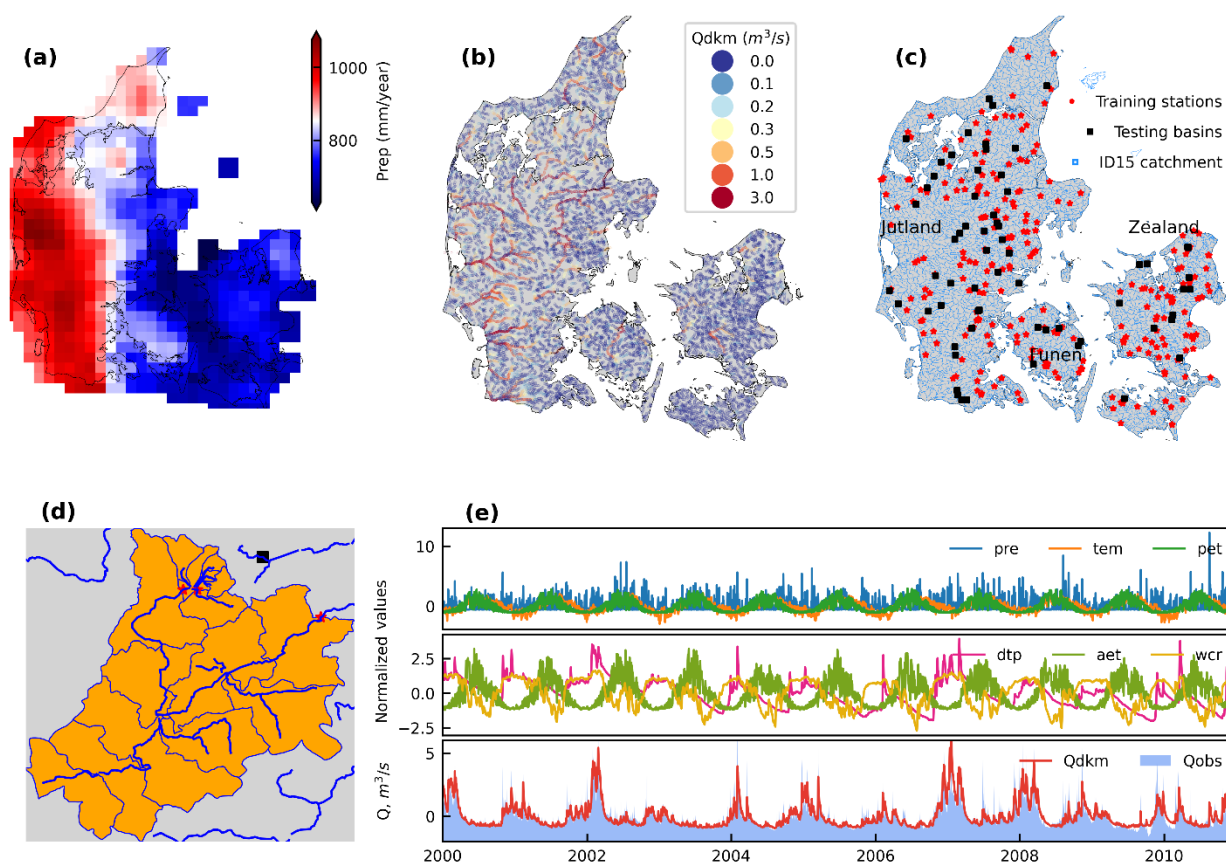
### 2.2.1 ID15 catchments

For various water management tasks, all of Denmark is subdivided into so-called ID15 catchments. Each ID15 catchment represents a topographic basin with an average area of about 15 km<sup>2</sup> (outlined in Fig. 1c). The total number of ID15 catchments is 3351. Out of these, 521 catchments lack a representation of the stream network in the DKM (mostly because they are small catchments draining directly to the sea) or located in small islands, which have been excluded in this study. With the selected 2830 ID15 catchment, we cover 90.60% of the land area of Denmark. Each of the catchments has data on flow direction and upstream/downstream catchments, allowing to obtain the total aggregated upstream area for all basins. Fig. 1c shows different scales of ID15 catchments, each of the shapefiles represents a catchment unit and connects with the upstream routing area. The catchment boundary to any required points on river networks is defined by identity index of the catchment unit. The ID15 catchments are connected with DKM discharge points (Q points), which are the grid points of the MIKE Hydro River setup where simulated discharge time series are available (DHI, 2020). Details of Q points will be described in the next section.

Based on the ID15 catchment dataset, we prepared a dataset of catchment attributes and hydrometeorological time series for the 2830 catchments, like the widely used CAMELS series dataset (Addor et al., 2017; Alvarez-Garreton et al., 2018; Chagas et al., 2020; Coxon et al., 2020; Fowler et al., 2021; Höge et al., 2023). The dataset includes static catchment attributes, dynamic variables of climate forcings, streamflow observations, and DKM simulations. Climate forcings have been described in the former section and include precipitation, temperature, and potential evapotranspiration. DKM simulated streamflow for each ID15 catchment was extracted from the Q points at the catchment outlets. The other simulations are grid-based spatiotemporally distributed variables originating from DKM at 500 m resolution, including actual evapotranspiration, average soil water content, and phreatic depth. They were all spatially aggregated into a time series for each ID15 catchment, including the entire upstream area. Fig. 2b shows all the Q points in the DKM with a total number over 48,000. Figure 2c shows the distribution of ID15 catchments and gauging stations. An example of spatially aggregated variables for a catchment in southeast Jutland is shown in Fig. 1d and Fig. 1e.

## 2.2.2 Climate forcings and basin attributes

The climate data used in this study includes precipitation, mean temperature, and potential evapotranspiration, which were  
160 obtained from the Danish Meteorological Institute (Scharling, 1999a, b). The temporal resolution of the climate data is daily,  
the spatial resolution of precipitation is 10 km and 20 km for both temperature and potential evapotranspiration. Precipitation  
was corrected based on daily wind speed and temperature to correct for precipitation sensor undercatch (Stisen et al., 2011).  
The climate forcings are used as inputs for both the DKM and LSTM models.



165

170

**Figure 1: Hydrometeorological characteristics of the study area. In the subplots, (a) shows the average annual precipitation in Denmark; (b) shows the average streamflow simulated by the DKM; (c) shows the ID15 catchments and the location of gauging stations which have been randomly divided into training (254 stations) and testing stations (64 stations) for LSTM model development; (d) shows the outline of a ID15 catchment (ID: 51350461, Vejle River) and the upstream subbasins which are also included in ID15 catchments; (e) shows spatially aggregated timeseries of the basin (ID: 51350461) during training period, including normalized precipitation (pre), temperature (tem) and potential evapotranspiration (pet), DKM simulated depth to phreatic surface (dtp), actual evapotranspiration (aet), and soil water content (wcr), DKM model simulated streamflow (Qdkm), and observed streamflow (Qobs).**



175 Catchment attributes, such as land use, soil type, topography, geology, and climate play a pivotal role in hydrological  
 modelling, as variations contribute significantly to the hydrological processes taking place in the basin. We selected 30 static  
 catchments attributes (Table 1) which we consider impacting the hydrological processes in Denmark. The spatial distribution  
 of these attributes is shown in Appendix A. The average elevation of all the catchments ranges from 0.10 m to 144.10 m with  
 a median elevation of 29.70 m. The median slope is 15.10% of all the catchments. The average clay content is higher in the  
 180 east than west Jutland. The static catchment attributes include simulation outputs from the DKM: the phreatic depth is included,  
 the median value is -1.91 m from a higher resolution DKM (100 m) and -1.55 m from a coarse resolution model (500 m)  
 (Schneider et al., 2022b; Koch et al., 2021). The spatial distribution of phreatic depth shows it is low in north and middle  
 Jutland. The median value of phreatic depth is -2.23 m in summer, and high in winter with a median value of -1.54 m.  
 Agriculture is the main land use type occupying 29.19%. Southern and central Jutland has a higher chalk aquifer depth, and  
 185 clay thickness above chalk aquifer.

**Table 1. Static catchment attributes**

Short name	Long name	Short name	Long name
Area	Catchment area	Urban	Fraction of urban
DEM	Digital elevation model (DEM)	Mean pre	Average precipitation
Slope	Slope calculated from DEM	Mean tem	Average temperature
Clay_tot_a	Average clay content across A horizon [%]	Mean pet	Average potential evapotranspiration
Clay_tot_b	Average clay content across B horizon [%]	Aridity	Ratio of mean PET to mean precipitation
Clay_tot_c	Average clay content across C horizon [%]	DKM_q	DKM simulated discharge
Clay_tot_d	Average clay content across D horizon [%]	DKM_aet	Actual evapotranspiration (500m model)
Dtp	Phreatic depth (100m model)	DKM_wcr	Average soil water content (500m model)
Dtp_s	Phreatic depth in summer (100m model)	DKM_dtp	Phreatic depth (500m model)
Dtp_w	Phreatic depth in Winter (100m model)	Clay depth	Depth of clay
Dtp_1m	1m exceedance probability of phreatic surface (100m model)	Depth CA	Depth to chalk aquifer
Dtp_2m	2m exceedance probability of phreatic surface (100m model)	Thick CA	Thickness of chalk aquifer
Agriculture	Fraction of agriculture	Clay thick CA	Clay thickness directly above chalk aquifer
Forest	Fraction of forest	Clay thick ACA	Accumulated clay thickness above chalk aquifer
Lake	Fraction of lakes	Chalk transm	Chalk transmissivity

### 2.2.3 Benchmark model 1 - the National Water Resources Model (DKM)

190 The DKM has been developed at the Geological Survey of Denmark and Greenland (GEUS) over the course of several decades  
 (Henriksen et al., 2021, 2003; Højberg et al., 2013; Soltani et al., 2021; Stisen et al., 2020). It is built on the MIKE SHE  
 hydrological modelling framework using a transient, fully distributed, physics-based description of the terrestrial hydrological  
 cycle (Højberg et al., 2013; Stisen et al., 2020; Abbott et al., 1986; DHI, 2020), 3D subsurface flow is coupled to processes in



the unsaturated zone, 2D overland flow and surface water routing in streams. The model is run with daily climate forcings  
195 (section 2.2.2) and is calibrated against daily streamflow observations from ~300 stations across Denmark (stations shown in  
Figure 1c), as well as groundwater head observations. It currently exists at two horizontal resolutions, 100m and 500m. For  
our case, we use the 500m version due to its reduced computational demand and the limited effect of enhanced grid resolution  
on streamflow simulations. For simulation of streamflow, MIKE SHE is coupled to the surface water model code MIKE Hydro  
River. In the case of the DKM, simple streamflow routing is applied as focus is on streamflow simulation (DHI, 2020). The  
200 MIKE SHE and MIKE Hydro River models are coupled through river links, where water is exchanged between river channel,  
land surface and subsurface. In the 500m version of the DKM, approximately 20,000 km of water courses are represented in  
this manner.

#### 2.2.4 Benchmark model 2 - LSTM rainfall-runoff model (LSTM-rr)

LSTM-rr uses meteorological forcings, including precipitation, temperature, and potential evapotranspiration as  
205 dynamic inputs, together with catchment attributes as embedded static inputs when the training and testing basins  
are more than one, and discharge observed at basin outlets as the target variable to develop the LSTM networks  
(Fuente et al., 2023; Hashemi et al., 2022; Koch and Schneider, 2022; Kratzert et al., 2021, 2018). The networks  
are usually trained and tested using historical data from a group of gauged basins and applied to extrapolate  
streamflow for unmonitored period or ungauged basins. LSTM-rr has gained popularity due to their ability to  
210 capture complex temporal dependencies and nonlinear relationships, and the predicted streamflow has often been  
found to outperform traditional hydrological models (Hauswirth et al., 2021; Frame et al., 2021a; Lees et al., 2021;  
Wilbrand et al., 2023; Feng et al., 2020).

### 2.3 LSTM hybrid schemes

We created four LSTM models distinguished by input sequences and target variables as the candidate hybrid model for  
215 streamflow simulations at national scale. The tested models include 1) pretraining-finetuning rainfall-runoff model, 2) dynamic  
inputs model with DKM simulations and climate forcing, 3) residual error prediction model, and 4) error factor prediction  
model. The first serves as benchmark to assess the accuracy that can be obtained by a standalone LSTM model without a hybrid  
scheme. The remaining four models represent different implementations of hybrid models. The following subsections describe  
the details of these models.

#### 2.3.1 Pretraining and finetuning LSTM rainfall-runoff model (LSTM-pf)

Pretraining and finetuning are techniques used to improve the performance of neural networks on specific tasks (MacNeil and  
Eliasmith, 2011; Käding et al., 2017; Cai and Peng, 2021). These techniques are commonly employed in transfer learning,  
where knowledge learned from one task or dataset is transferred to another related task or dataset (Li and Zhang, 2021; Tan et





al., 2018). Pretraining involves training a neural network on a large dataset or a related task before finetuning it for the target  
225 task. This helps the model learn useful features and representations from the large dataset and grasp general patterns of the  
data. Finetuning takes a pretrained neural network and further trains it on a smaller dataset specific to the target task, updating  
its weights accordingly. In this study, we pretrained an LSTM-rr model based on all ID15 catchments, climate forcings as  
dynamic inputs, basin attributes as static inputs, and DKM simulated streamflow as the target variable. This process enables  
the LSTM model to learn major features between climate data and the simulated discharge. Finetuning is then conducted on  
230 basins of observed discharge, i.e., the target variable is changed from DKM simulation discharge to observations. The  
hyperparameters are the same for both pretraining and finetuning. The total number of epochs is equivalent to that of LSTM-  
rr, with the first half is allocated for pretraining and the second half dedicated to fine-tuning.

### 2.3.2 Hybrid dynamic inputs LSTM model (LSTM-q)

In this configuration, the dynamic inputs are expanded with DKM simulations that impact river streamflow, including depth  
235 of the phreatic surface, average soil water content, actual evapotranspiration, and the DKM simulated streamflow itself. The  
depth to phreatic surface varies among basins with different hydrogeological properties, like permeability of the subsurface  
materials, aquifers, and confining layers. Groundwater pumping for irrigation, industrial use, or drinking water supply can  
significantly alter the interaction between phreatic surface depth and river discharge. Pumping can lead to a lowering of the  
groundwater table, reducing the groundwater contribution to river flow. DKM includes water extraction for drinking water  
240 supply and irrigation, thus, the variation of phreatic depth reflects the impacts of climate conditions and human activities.

### 2.3.3 LSTM residual error model (LSTM-qr)

Often, streamflow of a river exhibits strong seasonality due to changes in precipitation and temperature throughout the year.  
Simulated streamflow and their associated errors often exhibit systematic patterns such as overestimating baseflow or  
underestimating high flow during specific periods and rates. This occurs because of the limitations in model structures and  
245 parameters. The misfitting follows certain regular patterns that can potentially be identified through data-driven algorithms.  
Some studies attempted to predict the residuals between PBM simulated streamflow and observations (Cho and Kim, 2022;  
Konapala et al., 2020). They argue that the variabilities of residuals are lower in comparison to the variabilities of streamflow  
itself, and their results showed that the streamflow simulations could be improved after applying the predicted residuals to  
PBMs simulated streamflow.

250 However, special attention should be paid to the residual time series because data-driven methods cannot effectively learn or  
predict them when residuals consistently manifest as random noise. To test the whiteness of residuals between DKM  
simulations and observations, we therefore analyse the autocorrelation to ensure that the time series of residuals are not simply  
related to noise. Figure 2 illustrates an example of the residuals between simulated and observed streamflow on a daily scale  
at the station shown in the previous figure. The residuals were calculated by observed streamflow minus DKM simulations, so



255 a positive residual indicates that the DKM simulations are lower than observations. It can be observed in Figure 2a that the simulated streamflow is typically underestimated in winter (high-flow seasons) and overestimated in the warm seasons (low-flow seasons), consistently occurring every year. The autocorrelation figure reveals several spikes outside the 99% bounds, indicating that the time series of residuals are not white noise and could potentially be predicted by LSTM networks.

260

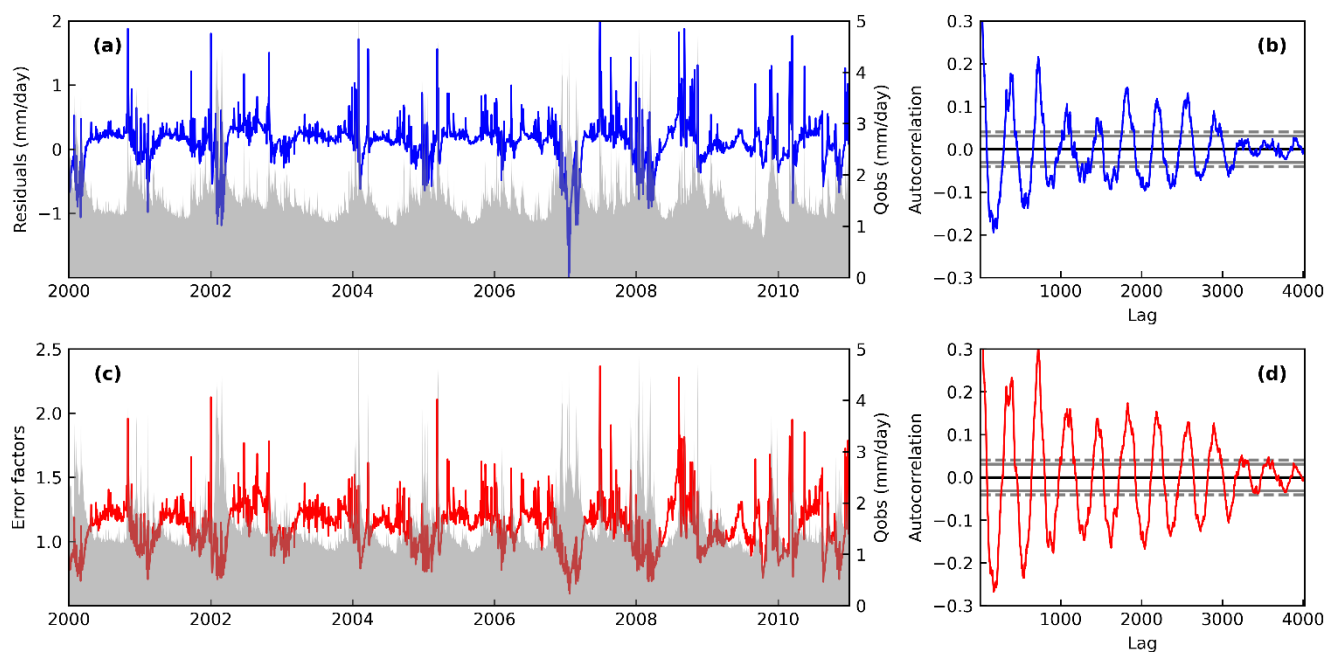


**Figure 2: Time series of streamflow residuals and error factors between DKM simulated streamflow and observations at a hydrological station (ID: 51350461). Autocorrelation of the time series are displayed in the second column to test white noise. The horizontal grey lines in the autocorrelation plots correspond to 95% (dash) and 99% (solid) confidence bands.**

265

### 2.3.4 LSTM error factor model (LSTM-qf)

The configurations of LSTM-qf are similar to LSTM-qr, but the target variables are relative error factors between observed streamflow and DKM simulations, instead of absolute residuals. The error factors were calculated by dividing observations with DKM simulations, so a value of 1 means DKM simulations are equal to observations. For example (Figure 2), we can see that DKM underestimates streamflow in winter when the precipitation is high and underestimates the streamflow in summer. Compared to streamflow residuals, error factors exhibit more variability and outliers (Figure 2c). The simulations are over 2 times lower than the observations during high flow events, which could be due to a mismatch in the peak-flow dates. For instance, the error factors are extremely high on one date and drop to values less than 1 on the following day, indicating a

270



275 mismatch in the peak-flow times. The plot shows that the error factors in time series are correlated and can be predicted by data-driven algorithms.

## 2.4 Experiment settings

To assess the potentials of various LSTM hybrid modelling schemes within both gauged and ungauged basins, we conducted a series of validation experiments. There are 318 gauged basins (Figure 1), which were randomly partitioned into training basins consisting of 254 stations (80%) and test basins comprising 64 stations (20%). Streamflow was divided into a training  
280 period from 2000 to 2010, the same as DKM calibration period, a testing period from 1990 to 1999, and a validation period from 2011 to 2019. We followed the design by Koch and Schneider (2022) and created temporal split experiments and spatiotemporal split experiments to evaluate the performance of LSTM models in gauged and ungauged basins. The temporal split experiment used the 254 training stations for training during the period from 2000 to 2010, and the same stations were used for testing during the test period from 1990 to 1999. The spatiotemporal split-sample experiment uses 254 stations for  
285 training during 2000 to 2010, and the trained model was tested on the 64 testing stations during 1990 to 1999.

The neuralhydrology python package is used to train and test all LSTM networks. The package is developed by Kratzert et al. (2022) and has been widely used in research after it was open-resourced (Frame et al., 2021b; Klotz et al., 2022; Koch and Schneider, 2022; Nearing et al., 2022; Wilbrand et al., 2023). All the LSTM hybrid schemes are trained with neuralhydrology package based on PyTorch on a server equipped with a NVIDIA A40 GPU (Paszke et al., 2019). The standard PyTorch  
290 implementation cudaLSTM in neuralhydrology package is used for LSTM training due to its efficiency. Dynamic inputs and static attributes are passed through embedding networks. The optimizer is Adam, and the loss function is Nash-Sutcliffe efficiency (NSE) for models with streamflow as target variable and root mean square errors (RMSE) for models with residuals or error factors as target variables.

295 **Table 2. The potential values of hyperparameters for LSTM models**

Hyperparameter	Number of epochs	Hidden unit size	Dropout rate	Batch size	Learning rate	Length of sequency
Potential values	[15, 20, 25, 30]	[64, 128, 256]	[0.1, 0.3, 0.5]	[128, 256, 512]	[ $10^{-3}$ , $5 \cdot 10^{-4}$ , $10^{-4}$ ]	[60, 90, 180, 365, 730]

Before using LSTM networks for specific tasks, it is necessary to determine the values of critical hyperparameters. Since there is no standard method to find an optimal set of hyperparameters for our case, we selected relevant hyperparameters based on  
300 previous studies and assessed their sensitivity (Cho and Kim, 2022; Hashemi et al., 2022; Kratzert et al., 2018). The selected hyperparameters include the number of training epochs, the size of hidden units, dropout rates, batch size, learning rates, and the lookback length of the sequence. The tested values for these hyperparameters are defined in Table 1. To assess the performance of all candidate hyperparameter combinations, a total of 1620 ( $4 \cdot 3 \cdot 3 \cdot 3 \cdot 3 \cdot 5$ ) possible combinations were generated. It is challenging to test all combinations for different LSTM models due to limited computational resources. Hence,



305 we randomly selected hyperparameters from the ranges listed in Table 2 and created 100 candidate hyperparameter combinations. The combination demonstrating the highest performance in terms of the average NSE values in the spatiotemporal split-sample experiment will be chosen to configure the final LSTM models. Table 3 shows the final hyperparameters for the LSTM models.

310 **Table 3. Optimal hyperparameters for LSTM models**

LSTM models	LL	HS	BC	LR	NE	DR
LSTM-rr	365	64	128	0.001	15	0.1
LSTM-q	90	256	128	0.001	25	0.5
LSTM-qr	365	64	128	0.001	15	0.3
LSTM-ql	365	256	128	0.001	15	0.5

\*NE: number of epochs, HS: size of hidden units, DR: dropout rate, BS: batch size, LR: learning rate, LL: length of lookback sequency.

## 2.5 Model evaluations

A set of statistical metrics is used to assess the performance of DKM and LSTM models (Table 3). These metrics have been widely used to compare the differences between simulated hydrography and observations (Baroni et al., 2019; Kratzert et al., 2018, 2021; Liu et al., 2022). NSE compares simulations to the average observations, quantifying the proportion of observed variance that the model can explain (Gupta and Kling, 2011). NSE ranges from negative infinity to 1, with 1 indicating a perfect match between model predictions and observations. Logarithmic NSE (NSElog) and squared NSE (NSE<sup>2</sup>) are two transformations of NSE; the former applies a logarithmic transformation to discharge before calculating NSE, while the latter applies a square transformation. NSE emphasizes errors associated with peak flows, NSE<sup>2</sup> amplifies extreme values and emphasizes the performance during peak flows even more (Schneider et al., 2022a). NSElog places higher emphasis on errors associated with low-flow situations (Roy et al., 2023). Kling-Gupta efficiency (KGE) combines three components: correlation, bias ratio, and variability ratio, which provides a balanced and comprehensive assessment of model performance. Root Mean Square Error (RMSE) measures the average magnitude of the differences between simulations and observations, which is suitable for the assessment extreme events modelling.

Further diagnostic signature measures are included to evaluate the performance of simulated streamflow. The high-segment volume (FHV) reflects the 2% peak flow bias of the flow duration curve, the low-segment volume (FLV) reflects 30% low flow bias, and the midsegment slope (FMS) reflects the percent bias of the midsegment slope of the flow duration curve. Peak-timing reflects the time difference between the simulated peak flow and the observed peak flow. Details about these signature measures are explained in Yilmaz et al. (2008), Gupta et al. (2009), and Kratzert et al. (2021). Table 3 displays the definitions and equations of the above-mentioned indices.



**Table 4. Overview of hydrography evaluation metrics**

Short name	Long name/ description	Range of values	Best fit value	Reference
NSE	Nash-Sutcliffe efficiency	$(-\infty, 1]$	1	Nash and Sutcliffe (1970)
KGE	Kling-Gupta efficiency	$(-\infty, 1]$	1	Gupta et al., (2009)
RMSE	Root Mean Square Error	$[0, +\infty)$	0	-
NSE <sub>log</sub>	Logarithmic NSE	$(-\infty, 1]$	1	Gupta et al., (2009)
NSE <sup>2</sup>	Square root NSE	$(-\infty, 1]$	1	Gupta et al., (2009)
FHV	High flow volume bias (2%)	$(-\infty, +\infty)$	0	Yilmaz et al., (2008)
FLV	Low flow volume bias (bottom 30%)	$(-\infty, +\infty)$	0	Yilmaz et al., (2008)
FMS	Middle flow slope bias (20% and 80%)	$(-\infty, +\infty)$	0	Yilmaz et al., (2008)
Peak timing	Mean peak time lag (in days)	$[0, +\infty)$	0	Kratzert et al., (2021)

335 **Table 5. Performance of DKM and the LSTM hybrid models in temporal split experiment and spatiotemporal split experiment (in bold).**

		Temporal split experiment						Spatiotemporal split experiment					
		DKM	LSTM-rr	LSTM-pf	LSTM-q	LSTM-qr	LSTM-qf	DKM	LSTM-rr	LSTM-pf	LSTM-q	LSTM-qr	LSTM-qf
NSE	Mean	0.58	0.80	0.72	0.80	0.81	0.77	0.52	0.59	0.52	0.63	0.63	0.62
	<b>Median</b>	<b>0.65</b>	<b>0.84</b>	<b>0.78</b>	<b>0.84</b>	<b>0.85</b>	<b>0.81</b>	<b>0.59</b>	<b>0.68</b>	<b>0.65</b>	<b>0.70</b>	<b>0.73</b>	<b>0.71</b>
KGE	Mean	0.65	0.78	0.70	0.81	0.83	0.80	0.59	0.61	0.54	0.65	0.64	0.65
	<b>Median</b>	<b>0.70</b>	<b>0.81</b>	<b>0.72</b>	<b>0.83</b>	<b>0.86</b>	<b>0.83</b>	<b>0.62</b>	<b>0.64</b>	<b>0.57</b>	<b>0.70</b>	<b>0.68</b>	<b>0.69</b>
NSE <sub>log</sub>	Mean	0.53	0.76	0.61	0.74	0.76	0.76	0.41	0.36	0.37	0.47	0.48	0.49
	<b>Median</b>	<b>0.66</b>	<b>0.82</b>	<b>0.69</b>	<b>0.80</b>	<b>0.83</b>	<b>0.81</b>	<b>0.58</b>	<b>0.63</b>	<b>0.49</b>	<b>0.61</b>	<b>0.66</b>	<b>0.63</b>
NSE <sup>2</sup>	Mean	0.12	0.65	0.57	0.65	0.64	0.52	0.15	0.46	0.38	0.46	0.43	0.44
	<b>Median</b>	<b>0.39</b>	<b>0.70</b>	<b>0.61</b>	<b>0.69</b>	<b>0.71</b>	<b>0.62</b>	<b>0.41</b>	<b>0.53</b>	<b>0.49</b>	<b>0.57</b>	<b>0.56</b>	<b>0.52</b>
FHV	Mean	0.44	-3.59	1.36	1.39	2.42	3.28	-0.74	-5.66	4.64	0.28	1.52	1.14
	<b>Median</b>	<b>0.36</b>	<b>-3.21</b>	<b>0.65</b>	<b>1.54</b>	<b>2.34</b>	<b>3.31</b>	<b>-1.32</b>	<b>-3.64</b>	<b>7.77</b>	<b>0.61</b>	<b>1.20</b>	<b>2.30</b>
FLV	Mean	108.23	47.62	144.82	91.56	47.57	57.11	84.23	63.96	139.02	127.60	52.97	73.75
	<b>Median</b>	<b>35.42</b>	<b>14.95</b>	<b>61.92</b>	<b>29.42</b>	<b>16.61</b>	<b>24.88</b>	<b>13.52</b>	<b>17.62</b>	<b>42.25</b>	<b>31.46</b>	<b>1.10</b>	<b>10.71</b>
FMS	Mean	-1.39	-10.65	-18.55	-13.20	-7.49	-9.87	7.13	-8.44	-16.50	-10.01	2.73	-4.24
	<b>Median</b>	<b>-6.53</b>	<b>-10.31</b>	<b>-20.21</b>	<b>-12.61</b>	<b>-8.46</b>	<b>-10.45</b>	<b>2.79</b>	<b>-18.17</b>	<b>-22.73</b>	<b>-19.09</b>	<b>-7.78</b>	<b>-8.35</b>
Peak timing	Mean	0.91	0.60	0.64	0.65	0.67	0.79	0.82	0.56	0.53	0.67	0.64	0.71
	<b>Median</b>	<b>0.80</b>	<b>0.56</b>	<b>0.56</b>	<b>0.58</b>	<b>0.60</b>	<b>0.69</b>	<b>0.79</b>	<b>0.43</b>	<b>0.44</b>	<b>0.53</b>	<b>0.57</b>	<b>0.64</b>

### 3 Results

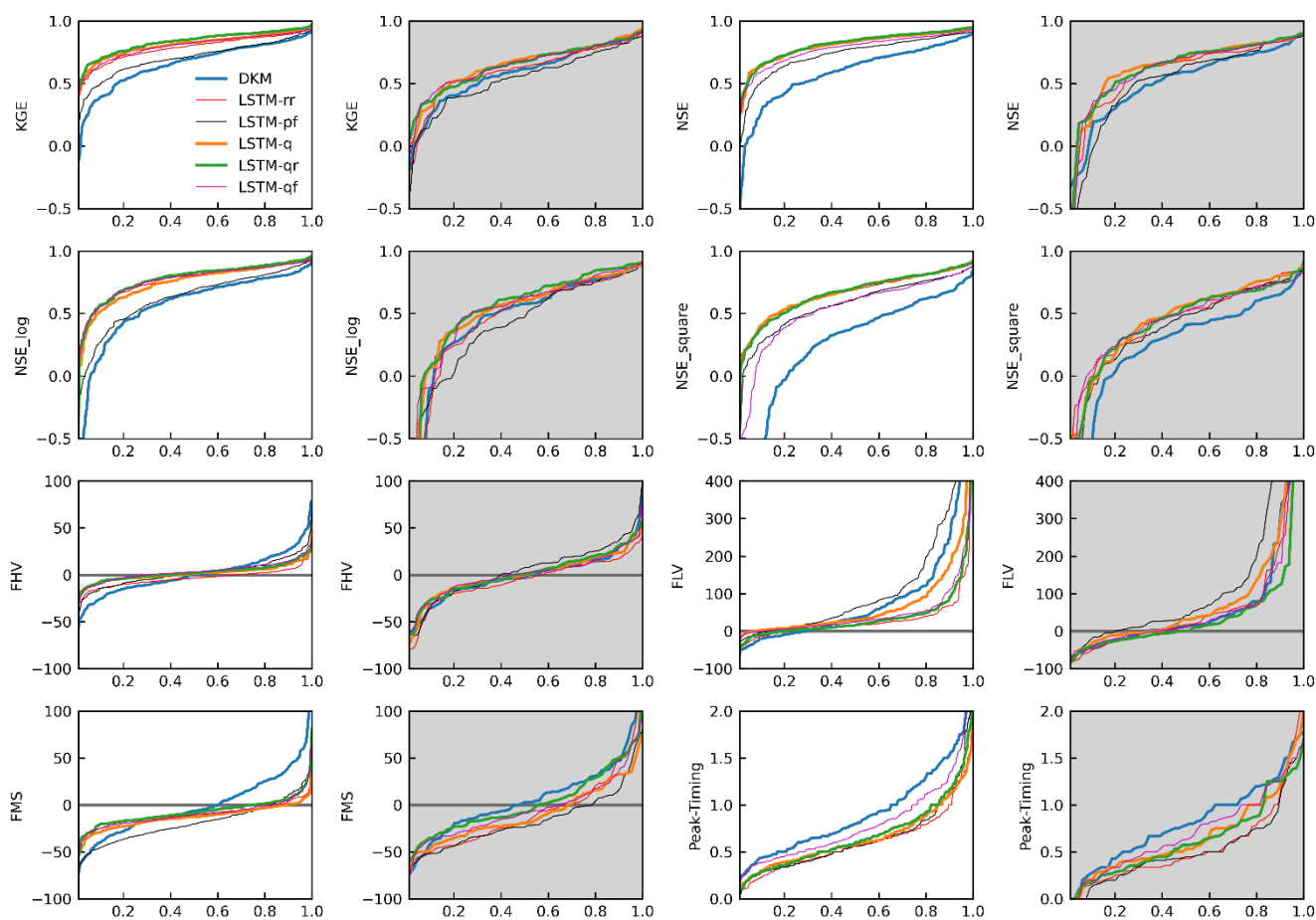
#### 3.1 Long-term performance of LSTM hybrid schemes

340 The cumulative distribution function (CDF) of evaluation metrics for the temporal split experiment (subplots with white backgrounds) and spatiotemporal split experiment (subplots with gray backgrounds) are shown in Fig. 3. Mean and median values of the evaluation metrics are listed in Table 5. In general, all LSTM models outperformed the DKM, underlining the potential of utilizing LSTM models for streamflow estimation. LSTM-qr (mean NSE is 0.81) exhibits the best model performance, closely followed by LSTM-q (median NSE is 0.80), LSTM-rr (0.80), LSTM-qf (0.77), and LSTM-pf (mean NSE is 0.73) in the temporal split experiment. LSTM hybrid models unaltered the performance significantly compared with the benchmark model LSTM-rr.

345 Performance of all LSTM models decreased when applied to ungauged basins, as revealed by the spatiotemporal split experiment. LSTM-q slightly outperforms LSTM-qr according to NSE and NSE<sup>2</sup> in the spatiotemporal split experiments, indicating that LSTM-q is more effective for high-flow modelling. This is further supported by FHV, which measures the bias



350 of peak flow where LSTM-q shows a lower error compared to LSTM-residual. In contrast, LSTM-qr demonstrates higher performance at low flows conditions with higher NSElog and lower FLV bias. The DKM model exhibits a higher peak timing error, while LSTM-rr shows the lowest peak timing error. LSTM-rr shows a lower NSElog than DKM, LSTM-q, and LSTM-qr, indicating its accuracy over low flow is poorer.



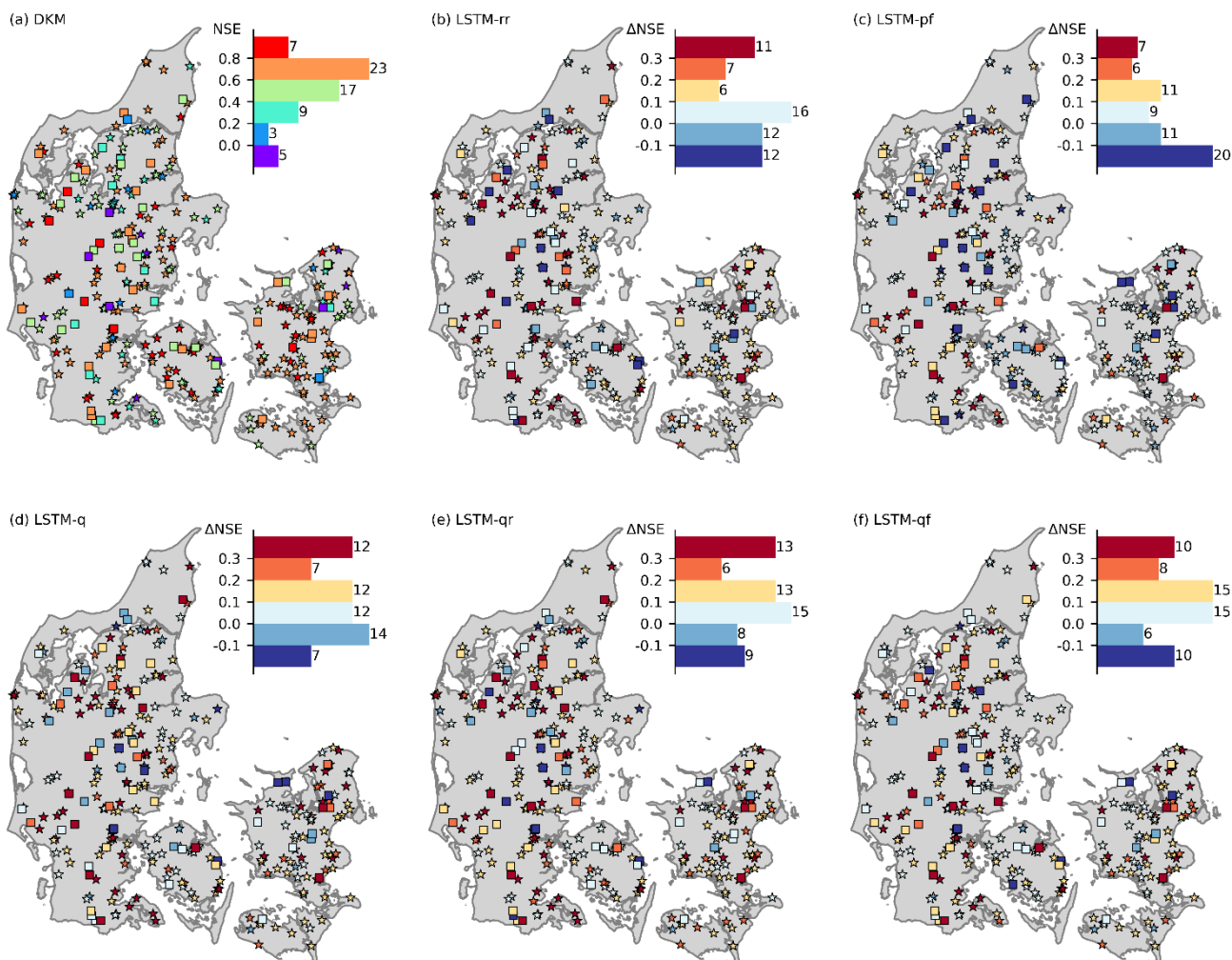
355

**Figure 3: Performance of benchmark models and LSTM hybrid models in temporal split experiment (subplots with white background) and spatiotemporal split experiment (subplots with grey background).**

Figure 4 shows the spatial distribution of NSE of DKM at all stations and the enhancements in NSE achieved by LSTM hybrid  
 360 modelling. DKM exhibits satisfactory performance in most basins, only seven stations from the temporal split experiment (out of 254 total) and five stations (out of 64 total) from the spatiotemporal split experiment display a negative NSE. DKM has difficulties in modelling streamflow in basins covered by large lake areas (Fig. 4), such as stations situated in central Jutland and northeast Zealand. LSTM hybrid models have improved NSE at many stations, as illustrated in the histogram in Fig. 4b-



f. Specifically, LSTM-rr has shown improved NSE at 40 stations in the spatiotemporal split experiment, LSTM-q improved 43 stations, LSTM-qr improved 47 stations, and LSTM-factor improved 48 stations. However, LSTM hybrid schemes still fail to enhance NSE at some stations, such as 24 stations for LSTM-rr, 21 stations for LSTM-q, and 17 stations for LSTM-residuals.



370 **Figure 4: Performance of DKM and LSTM models during the testing period (1990-1999) of temporal split experiment (marked by star) and spatiotemporal split experiments (marked by square). (a) NSE of DKM. The histogram can be understood as legend to the map and the width bars indicate the number of testing stations in corresponding ranges of NSE. (b – f) shows the differences of NSE between DKM and LSTM ( $\Delta NSE = NSE_{LSTM} - NSE_{DKM}$ ). The histogram can be understood as legend to the map and the bars indicate the number of testing stations in corresponding ranges of ΔNSE.**

375 Figure 5 presents the time series of streamflow for two example stations from the spatiotemporal split experiment located in the central Jutland, which we have named basin A (ID=13261645) and basin B (ID=35324466). The DKM model



overestimates high-flow periods and underestimates low-flow periods in basin A, resulting in a negative NSE. LSTM-rr agrees well with observations during high-flow seasons but tends to overestimate during low-flow periods. The simulated hydrograph of the LSTM hybrid models, falls between the ranges of DKM and LSTM-rr, indicating superior performance compared to  
380 DKM and LSTM-rr. However, the finding differs in basin B, where DKM-simulated streamflow aligns well with observations, and NSE exceeds 0.6. Basin B is spatially close to basin A, and the climate forcings are equivalent. We then compared the basin attributes of basins A and B with those of the basins used for LSTM training. The slope of basin B (5.03) is significantly higher than that of basin A (1.14) and most training basins (ranging from 0.258 to 4.580). The forest ratio of basin B is 27.61%, whereas it is 5.98% for basin A. These distinct differences between basin A and the training dataset result in the inferior  
385 performance of LSTM models. These results demonstrate the challenges of extrapolating streamflow to ungauged basins and the importance of selecting training datasets with diverse catchment attributes.

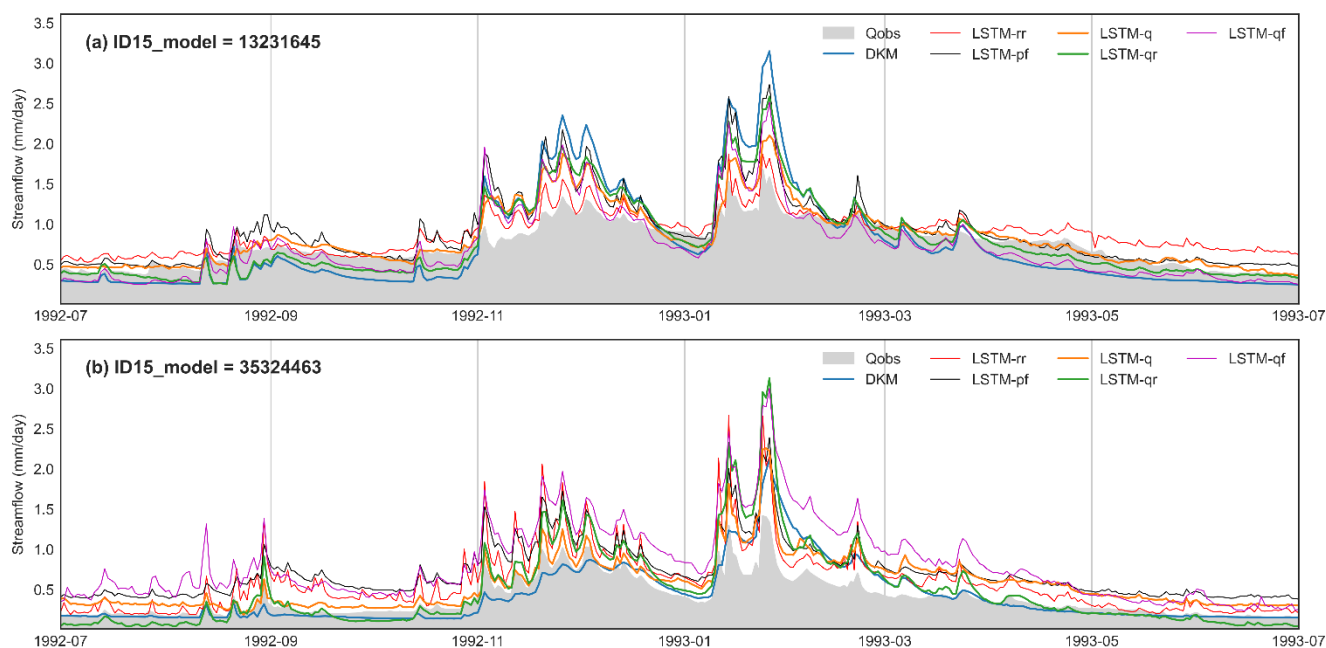


**Figure 5: Time series of streamflow at two hydrological stations which was involved in the spatiotemporal split experiment.**

390

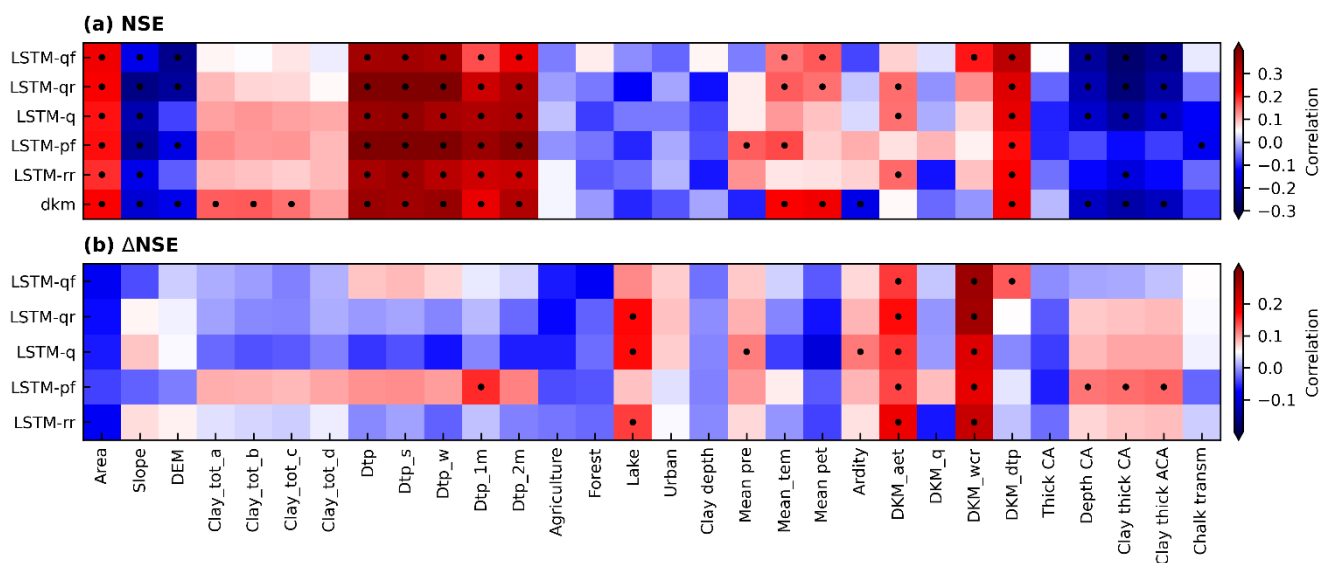
Fig. 6 presents a heatmap of correlation coefficients between model performance (NSE and  $\Delta$ NSE) of the different models and static basin attributes. Unsurprisingly, basin area positively correlates with all models' performance, i.e., performance generally is better for larger basins. DKM simulated groundwater levels (dtp, dtp\_s, dtp\_w, dtp\_1m, and dtp\_2m) positively correlate with NSE for all models, indicating that the models generally struggle to accurately simulate streamflow in basins with deeper groundwater levels. In Denmark, much of the streamflow is generated as baseflow; thus, controlled by groundwater  
395 levels. With deeper groundwater levels, accurate representation of groundwater level dynamics becomes more challenging.





The negative correlation between model performance and the share of lake area can be explained by the complex interactions in lake water balances; something both the DKM and the LSTM models struggle with. Similarly, increased urban share decreases model performance; again, likely due to complexities and heterogeneities in urban hydrology inadequately represented in the models. Geological features such as depth to the chalk aquifer, clay thickness above the chalk aquifer, and accumulated clay thickness above the chalk aquifer negatively correlate with the performance of both DKM and LSTM models. The reasons for this require further investigation.

The changes in performance of the LSTM models compared to the DKM ( $\Delta NSE$ ) exhibit a negative correlation with basin area, suggesting that LSTM model improvements decrease with increasing basin size (Fig. 6b). This might be related to all basin information being aggregated across each basin for the LSTM models, whereas the distributed nature of the DKM allows representation of more complex streamflow generation processes (and routing) within basins.  $\Delta NSE$  indicates a positive correlation with DKM\_wcr and DKM\_aet, both showing similar spatial patterns (refer to Appendix A), signifying improved performance of LSTM models over DKM in, generally speaking, basins with higher soil moisture. In such basins, runoff generation might be more driven by complex hydrological and land-surface processes e.g. occurring in wetlands, instead of more simply being driven by precipitation. The description of such land-surface processes in the DKM, where the simple “2-Layer-method” is being used, are inadequate for capturing some complexities (DHI, 2020; Yan and Smith, 1994). Similarly, the LSTM models show performance improvements for catchments with higher share of lake areas. Again, the representation of lake water balances and streamflow through lakes is one of the weaknesses of the DKM.



415 **Figure 6: Correlations between the performance (NSE) and changes in performance ( $\Delta NSE = NSE_{lstm} - NSE_{dkm}$ ) of different LSTM models and catchment static attributes. The black points indicate the correlations pass the 95% significant tests.**



### 3.2 Events performance of LSTM hybrid schemes

The objective of developing different LSTM models is to identify an optimal hybrid scheme to support the operational modelling and forecasting framework, which the DKM is already a part of. A real-time module has been established to collect daily observations of climate forcings, including precipitation, temperature, and potential evapotranspiration, which serve as inputs for a real-time DKM. Within the operational real-time framework, emphasis is placed on modelling extreme events. Therefore, in this section, we investigate the performance of LSTM hybrid schemes in modelling extremely high and low flows.

We selected four distinct wet periods characterized by high peak flows across many regions of Denmark, as well as two dry periods marked by severe drought conditions. Figure 7 displays the observed streamflow and simulations from the DKM, LSTM-q, and LSTM-qr averaged across all stations, as well as the histogram of RMSE for all stations. The two LSTM hybrid models (chosen based on their superior performance) show improved RMSE compared to the DKM at most stations but fail at a few stations as indicated by the tail of the fitted frequency density curve (Fig. 7a). Capturing peak flows accurately proves challenging for both DKM and the LSTM hybrid schemes, as the simulated streamflow values tend to be lower than observations during the four flooding events.

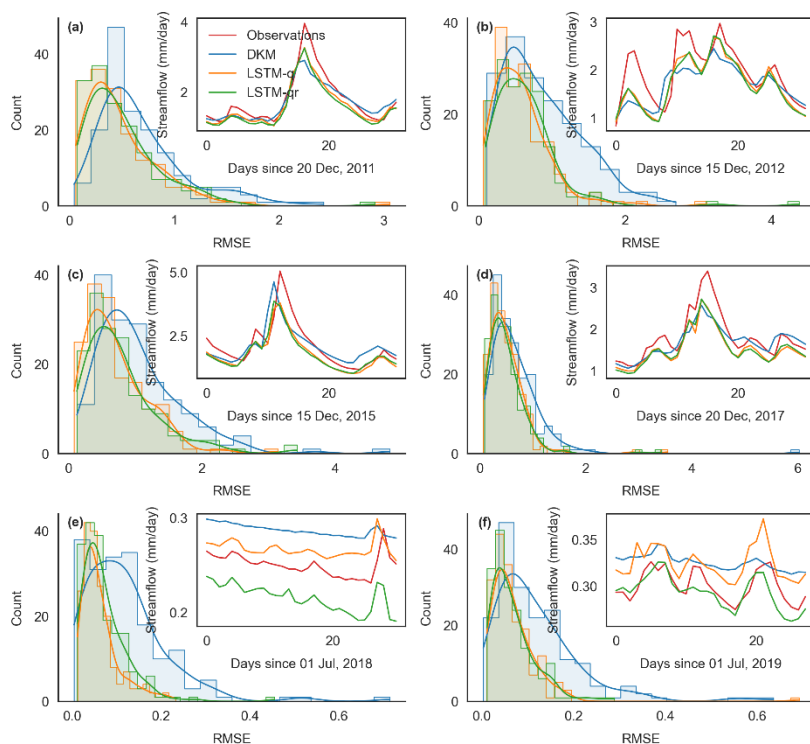
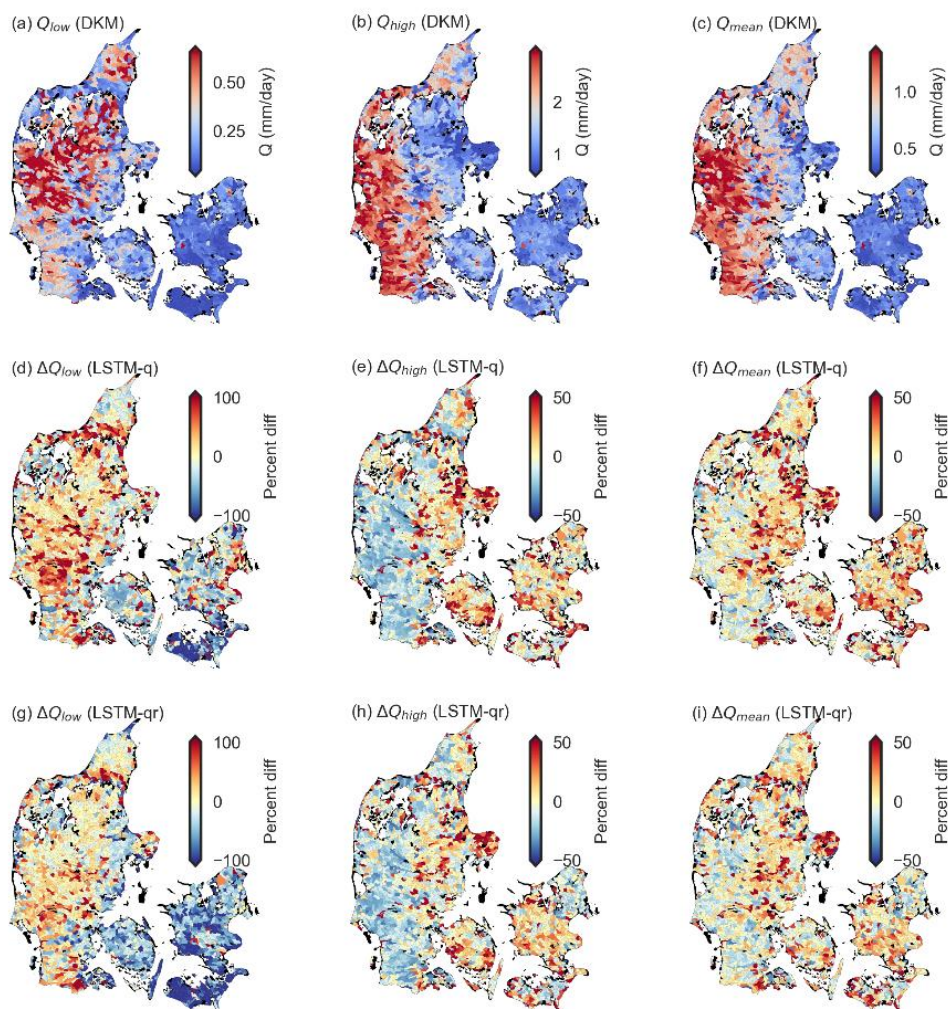


Figure 7: Performance of DKM, LSTM-q, LSTM-qr during extreme events. (a - d) four flooding events, and (e -f) two drought events. In each subplot, the main figure shows the histogram of RMSE calculated across all stations and the fitted probability density function, an additional figure in the top-right shows the averaged time series of streamflow.



### 3.3 Comparison of LSTM models and DKM at a national level

After developing and identifying the optimal LSTM hybrid schemes, we extended their application from predicting streamflow in gauged basins to ungauged basins, such as the outlets of all ID15 catchments across Denmark. Fig. 8 illustrates the high/median/low flow of DKM in all ID15 catchments from 2010 to 2020, the residuals between LSTM-q and DKM, and the residuals predicted by LSTM-qr in all ID15 catchments. DKM and LSTM models generally agree well with each other in most basins, with percentage differences close to 0. This further underlines the robustness of the LSTM models, also in spatial extrapolation, as they manage to follow the simulated streamflow patterns from the DKM which is based on a spatially consistent setup, calibrated jointly for all of Denmark. However, discrepancies arise in certain basins, as indicated by deep red and deep blue colours, particularly during high and low flow conditions. In Jutland, the LSTM models tend to simulate higher low flows compared to DKM, while in Zealand and Funen, the opposite pattern is observable. In western Jutland, where precipitation is higher and DKM-simulated streamflow is larger than in other regions, the LSTM models predict lower high flows. DKM overestimate high flows, and reducing the value of DKM simulations can enhance accuracy in these cases.



450

**Figure 8: A comparison of simulated streamflow differences between DKM and two LSTM models (LSTM-q and LSTM-residual). The first row depicts DKM simulated streamflow during high flow, low flow, and median flow conditions, the second row is the bias between DKM simulations and the LSTM-q predictions, and the third row is the bias between DKM and LSTM-qr. The percent diff in the figure is defined as the differences between LSTM model and the DKM,  $\text{percent diff} = (Q_{LSTM} - Q_{DKM}) \times 100$ .**

455

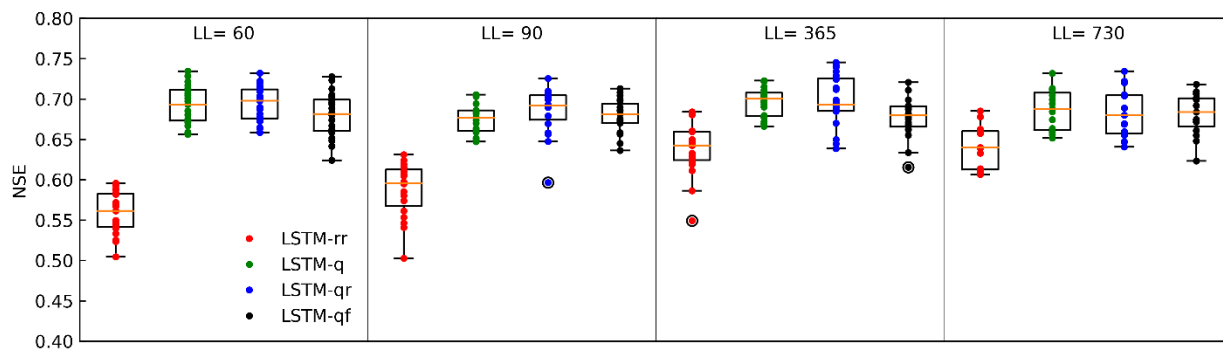
#### 4 Discussion

In this study, a series of experiments were conducted to enhance the performance of streamflow estimation at national scale in Denmark. The main objective was to assess various configurations of LSTM models to identify the optimal configuration to serve as a hybrid model for streamflow prediction. The results revealed that utilizing LSTM models, especially the hybrid



460 schemes that were coupled with physically based simulations, exhibited superior performance for both long-term periods (spanning a decade) and short-term extreme events (30 days).

Overall, we found that the trained LSTM models were robust, and their performance was relatively consistent across the tested hyperparameters. Figure 9 underlines that the variations of NSE across the sensitivity analysis of 100 hyperparameter combinations are small. Previous studies often applied default hyperparameters for LSTM development, a practice that remains  
465 justifiable due to the generally limited impact of hyperparameter adjustments. However, it is necessary to mention that the robustness of LSTM models can be further enhanced through the incorporation of physical knowledge into the selection of hyperparameters. For instance, the selection of a lookback length for sequential time series data traditionally adheres to 365 days for LSTM rainfall-runoff models, a choice made to account for the seasonal dynamics in hydrological processes. Nevertheless, the lookback length can be reduced to under three months in the hybrid modelling schemes, as model  
470 performance remains reliably consistent across these diverse temporal scales. This suggests that in this case, the longer-term hydrological information is contained in the PBM outputs such as groundwater levels. Conversely, we find that the LSTM-rr model, without the DKM as input, benefits from a prolonged lookback length.



475 **Figure 9: The relationship between NSE and sequential lookback length (LL) of the spatiotemporal split experiment.**

The design of the applied temporal split experiment and spatiotemporal split experiment aimed at illustrating the potential performance of LSTM models in gauged and ungauged basins. In this study, the performance of LSTM models ( $NSE > 0.8$ ) in gauged basins are comparable to previous studies (Cho and Kim, 2022; Lees et al., 2021; Konapala et al., 2020; Frame et al., 2021c). The performance dropped for ungauged basins (spatiotemporal split experiment in Fig. 3), well aligned with (Koch and Schneider, 2022). Few studies conducted a comparable spatiotemporal hold-out experiment, thus special attention should be paid to validate the performance of LSTM models over ungauged basins. For example, Kratzert et al. (2019b) applied a 12-fold cross validation experiment over the contiguous United States and found a limited drop in performance for the predictions in ungauged basins. However, the applied 8.3% spatial holdout may not pose the most challenging validation test. In our study,



485 we applied a larger 20% spatial hold-out and a more systematic k-fold validation test was hampered by inconsistent length of observations across the Danish discharge stations.

The intricate interactions between groundwater and surface water have posed challenges for simulating streamflow using rainfall-runoff models in many basins of Denmark (Danapour et al., 2019; Duque et al., 2023). We tested LSTM-rr for streamflow estimation, and the results were encouraging, with the mean Nash-Sutcliffe Efficiency (NSE) improving from 0.58 (DKM) to 0.80 (Table 5). These improvements indicate the large potential of LSTM-rr model for streamflow modelling. However, it is important to note that LSTM-rr may not perform well everywhere, as evidenced by its limitations in strongly groundwater dependent regions, such as northern Jutland. LSTM-rr simulates quick responses to the variations of precipitation well but can fail to predict reduced baseflows due to depleted groundwater storage (Fig. 5a). Also, the performance drop between temporal and spatiotemporal holdout is most pronounced for LSTM-rr (NSE is reduced from 0.80 to 0.59). Therefore, 490 it is important to emphasize the advantages of integrating physical data into the LSTM framework, and the adoption of hybrid schemes, such as LSTM-q and LSTM-qr, yielded improvements in the estimation of streamflow. These results align with the findings of previous studies (Feng et al., 2022; Frame et al., 2021c; Hunt et al., 2022; Zhang et al., 2023; Cho and Kim, 2022; Konapala et al., 2020; Tang et al., 2023) that assessed the potential of hybrid modelling.

We tested four different hybrid systems: LSTM-pf, LSTM-q, LSTM-qr, and LSTM-qp. They all exhibited satisfactory 500 performance for streamflow estimation according to the evaluation metrics, with the order of priority (from high to low) being LSTM-qr  $\approx$  LSTM-q  $>$  LSTM-rr  $>$  LSTM-qp  $>$  LSTM-pf  $\approx$  DKM. The better performance of LSTM-q is consistent with previous studies, for instance, Cho and Kim, (2022) proved that WRF-Hydro-LSTM has a lower percent bias than LSTM-rr. Tang et al. (2023), Frame et al. (2021b), and Hunt et al. (2022) showed that LSTM models with additional datasets of hydrological signals as inputs as well as simulations of global hydrological models outperformed LSTM-rr. However, our 505 finding that LSTM-qr is slightly better than LSTM-q differs from Konapala et al., (2020). They pointed out that the LSTM-qr model was inferior to LSTM-q across the conterminous US. In their work, LSTM-qr showed comparable performance with LSTM-q when the NSE of PBM was larger than 0.75, and the improvement of LSTM-qr then decreased as the NSE of PBM decreased. Thus, the performance of LSTM-qr was overly constrained by the performance of the underlying PBM, whereas the LSTM-q was found to be more flexible. In our study, DKM performs better than the PBM in Konapala et al., (2020), and 510 27% of the stations have an NSE higher than 0.75, whereas the percentage is 18% in their study. Thus, this can explain the slightly increasing performance of LSTM-qr compared with LSTM-q in our case, because the underlying PBM, the DKM, performs generally very well. Additionally, the performance of LSTM-pf is not comparable to the other LSTM hybrid schemes, which differs from the conclusion of Koch and Schneider (2022). This can be explained by the fact that in the pre-training, the model is pre-trained against DKM simulated streamflow from all 2830 ID15 catchments as the target variable, whereas the 515 finetuning is performed against only the observation station data. This may introduce more complexity and noise for LSTM to learn. Koch and Schneider (2022) only pre-trained using simulated DKM based streamflow at the same basin where observations were available. We also implemented an experiment that pre-trained a model on gauged basins only with DKM simulated streamflow as target variables, then finetuning the model with observations, and the performance is comparable to



LSTM-rr. To our knowledge, LSTM-qf is a novel hybrid modelling scheme, tested for the first time in the present study. The  
520 performance of LSTM-qf is lower than LSTM-qr. This is likely related to the use of DKM simulated streamflow as  
denominator when calculating the error factors, which can be problematic if simulated streamflow is close to zero resulting in  
large and instable factors. Figure 2 shows that the variability of error factors is larger with more outliers than residual time  
series. Thereby, we recommend for future work to focus on the residual approach instead of the factor approach.

We intended to train a skillful LSTM model to be used to forecast discharge across Denmark in an operational real-time  
525 framework, currently under development. However, the LSTM networks presented in this study have shallow structures and  
trained against a limited number of gauged basins, limiting their ability to capture some features deeply hidden in the  
hydrometeorological time series and catchments attributes. The catchments have a large variety of static attributes spatially,  
and the hydrological regimes change significantly across Denmark. The hybrid schemes alleviated the shallow structures as  
discussed above, other solutions could be enhancing the complexity of the neural networks, and developing specific DL models  
530 for different regions distinguished by regime information (Hashemi et al., 2022).

Spatially, we predicted streamflow at a large number of catchments, namely 2830 outlets, covering most of Denmark. The  
comparison of LSTM and PBM performance across the entire region gives some insights in controlling factors on the different  
models' performance, potentially guiding further model improvement (especially of the PBM). Another question that arises in  
this case of nested catchments is how LSTM models can be developed that produce consistent streamflow simulations along  
535 river courses, with as many Q points as distributed hydrological models. This is particularly useful, as many PBMs currently  
provide streamflow simulations at explicit grids or points within the catchment (Harrigan et al., 2023). Correcting the  
streamflow at each PBM simulation point offers advantages, such as improving the prediction of local flooding extent,  
assessing drought hazards, and estimating nitrate transport, all of which require a refined resolution of streamflow at local  
scales. This is why LSTM-qr and LSTM-qf hybrid schemes were considered in this study, which can be predicted at the basin  
540 outlets and, potentially, can be applied to all Q-points within a subbasin. Ideally, discharge routing in the river channel involves  
linear accumulation from upstream to downstream and therefore, we can use relative residuals or error factors not only at basin  
outlets but also for upstream locations. However, implementing such an idea is challenging, given that river routing processes  
do not change linearly from upstream to downstream due to additional water from small tributaries, groundwater contributions,  
and river regulation. Further information on river routing and the relationship of streamflow between upstream Q points and  
545 outlets should be considered, and advanced methods should be investigated for distributing residuals and error factors to all  
the Q points upstream. On the other hand, the development of distributed LSTM rainfall-runoff models or distributed LSTM  
hybrid schemes could be a new topic in the future.

## 5 Conclusion

This study aimed at identifying optimal LSTM hybrid schemes based on the National Water Resources Model (DKM) to  
550 enhance streamflow estimation at a national scale. To achieve this, we developed four LSTM hybrid models with varying



dynamic inputs and target variables, evaluating them under different scenarios, including temporal and spatiotemporal split experiments. Two optimal LSTM models, LSTM-q and LSTM-qr, were further assessed for their performance in extreme events. Lastly, we compared the disparities between DKM and the optimal LSTM models, seeking insights into hydrological modelling from both perspectives. The key conclusions of this study are:

555 (1) LSTM models excel at modelling streamflow in Denmark, demonstrating superior performance compared to DKM. The LSTM-rr model performs satisfactorily in numerous basins, with a mean NSE of 0.80 in the temporal split experiment and 0.59 in the spatiotemporal split experiment. However, it faces challenges in simulating streamflow in groundwater-dominant regions as well as spatial transferability, which can be mitigated by employing hybrid LSTM models.

(2) The best-performing hybrid models are LSTM-qr and LSTM-q, achieving mean NSE values of 0.80 and 0.81, respectively. 560 Also, in ungauged basins they surpass the DKM performance, with a mean NSE of 0.63, compared to 0.52 of the DKM. In the spatiotemporal split experiment, LSTM-qr improved the accuracy compared to the DKM for 73% of stations, while LSTM-q improved 67%. Basin attributes such as catchment area, average clay content, and phreatic depth correlate positively with model performance, whereas factors like slope, DEM, lake ratio, depth, and clay thickness related to chalk aquifers correlate negatively with model performance.

565 (3) LSTM hybrid models also contribute to improving the modelling of extreme events. LSTM-qr and LSTM-q effectively reduce errors in DKM simulated values during high and low-flow periods in Denmark. But still, more efforts should be made to improve the modelling accuracy toward extreme values in the hydrographs, considering LSTM models underestimate the peak flow of flooding events.

The utilization of LSTM in river streamflow modelling heralds a promising perspective for hydrological predictions. Previous 570 studies focused more on gauged basins, while this study contributes to the topic with a national scale analysis. We found that the conventional LSTM-rr model has limited performance in regions with complex hydrological processes. Information from physical hydrological models is helpful, as indicated by the benefits across several hybrid schemes. Our future plans include evaluating the hybrid schemes in a real-time forecasting framework forced by forecasted climate data and developing distributed LSTM hybrid schemes.

575

*Code and data availability.* The LSTM code used in this study is based on the neuralhydrology Python package, which can be accessed via <https://neuralhydrology.github.io>. Upon request, the corresponding author will provide scripts for data preprocessing, post-processing, and visualization. The climate forcings and DKM simulations, as well as the in-situ observations used in this study, are currently being organized for publication and are available upon request prior of publication 580 of the data paper.

*Author contributions.* All authors contributed to develop the original idea and design experiments. JL conducted the experiments, in close cooperation with RS and JK, and further inputs from SS and LT. The code for data preprocessing, LSTM





training and testing, data post-processing and visualization were prepared by JL with support by RS and JK. JL and RS prepared  
585 the manuscript, with contributions from JK, SS, and LT. All authors were involved in writing the manuscript.

*Competing interests.* The authors declared that there are no competing interests.

590 *Acknowledgements.* The work presented in this manuscript was performed to enhance flood warning for Denmark as part of  
the establishment of the Danish flood warning system (varslingssystem for oversvømmelser) from 2023 to 2026. The project  
is being led by the Danish Meteorological Institute (DMI), in cooperation with the Geological Survey of Denmark and  
Greenland (GEUS), the Danish Agency for Data Supply and Infrastructure (SDFI), the Danish EPA (MST), the Danish Coastal  
Authority (KDI) and the Danish Environmental Portal (DMP). Special thanks are due to Anker Lajer Højberg for providing  
595 the shapefile of ID15 catchments, and to Mark F. T. Hansen for verifying the connection between the ID15 catchments and  
DKM.

Appendix A

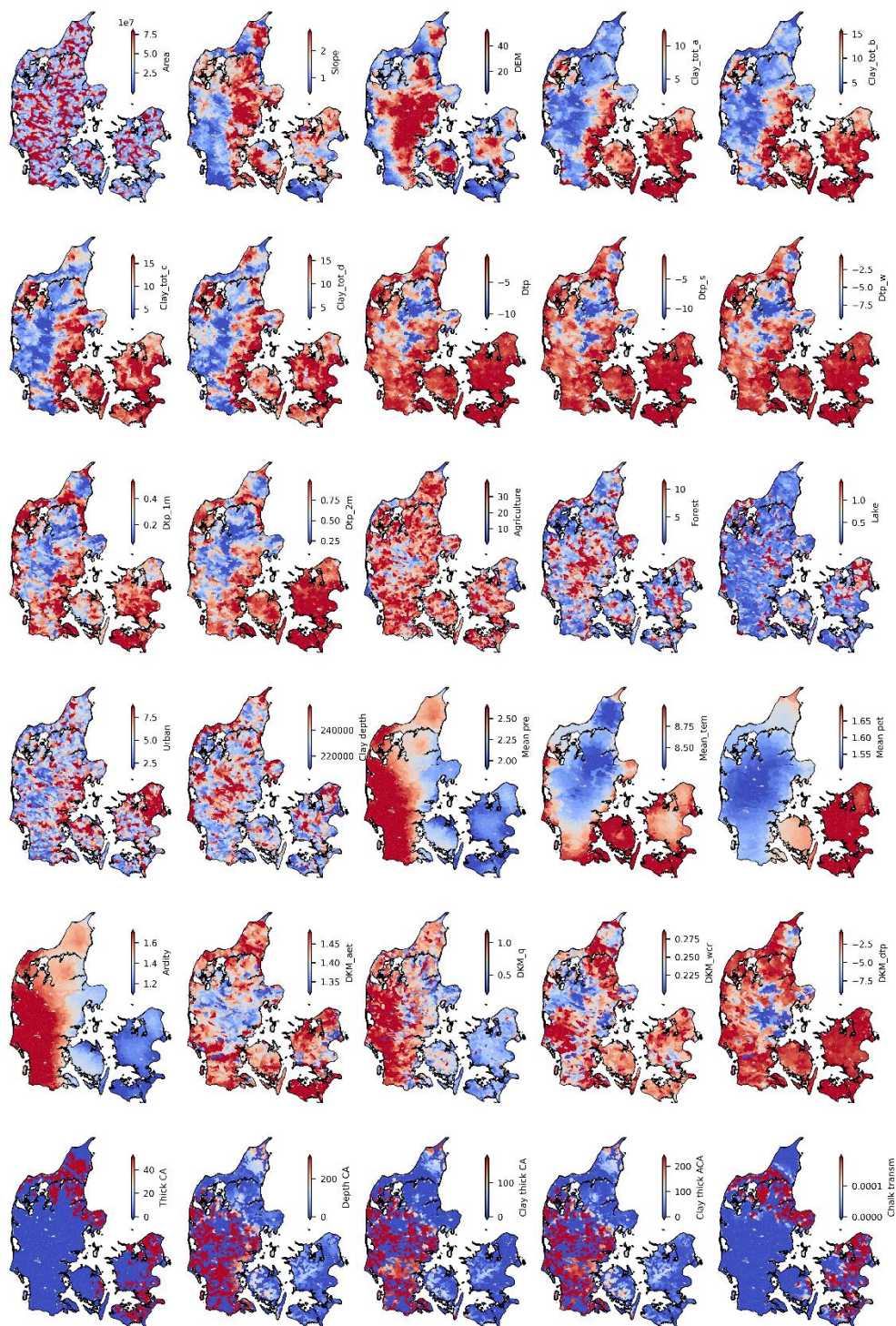


Figure A1. Distribution of catchment attributes.



## References

- Abbott, M. B., Bathurst, J. C., Cunge, J. A., O'Connell, P. E., and Rasmussen, J.: An introduction to the European Hydrological System — Systeme Hydrologique Europeen, “SHE”, 1: History and philosophy of a physically-based, distributed modelling system, *J. Hydrol.*, 87, 45–59, [https://doi.org/10.1016/0022-1694\(86\)90114-9](https://doi.org/10.1016/0022-1694(86)90114-9), 1986.
- 605 Addor, N., Newman, A. J., Mizukami, N., and Clark, M. P.: The CAMELS data set: Catchment attributes and meteorology for large-sample studies, *Hydrol. Earth Syst. Sci.*, 21, 5293–5313, <https://doi.org/10.5194/hess-21-5293-2017>, 2017.
- Alvarez-Garreton, C., Mendoza, P. A., Pablo Boisier, J., Addor, N., Galleguillos, M., Zambrano-Bigiarini, M., Lara, A., Puelma, C., Cortes, G., Garreaud, R., McPhee, J., and Ayala, A.: The CAMELS-CL dataset: Catchment attributes and meteorology for large sample studies-Chile dataset, *Hydrol. Earth Syst. Sci.*, 22, 5817–5846, <https://doi.org/10.5194/hess-22-5817-2018>, 2018.
- 610 Amendola, M., Arcucci, R., Mottet, L., Casas, C. Q., Fan, S., Pain, C., Linden, P., and Guo, Y.-K.: Data Assimilation in the Latent Space of a Neural Network, 2020.
- Arsenault, R., Martel, J. L., Brunet, F., Brissette, F., and Mai, J.: Continuous streamflow prediction in ungauged basins: Long short-Term memory neural networks clearly outperform traditional hydrological models, *Hydrol. Earth Syst. Sci.*, 27, 139–157, <https://doi.org/10.5194/hess-27-139-2023>, 2023.
- 615 Baroni, G., Schalge, B., Rakovec, O., Kumar, R., Schüler, L., Samaniego, L., Simmer, C., and Attinger, S.: A Comprehensive Distributed Hydrological Modeling Intercomparison to Support Process Representation and Data Collection Strategies, *Water Resour. Res.*, 990–1010, <https://doi.org/10.1029/2018WR023941>, 2019.
- 620 Beven, K.: How to make advances in hydrological modelling, *Hydrol. Adv. Theory Pract.*, 1969, 19–32, <https://doi.org/10.2166/nh.2019.134>, 2020.
- Beven, K. J.: A discussion of distributed hydrological modelling, in: *Distributed hydrological modelling*, Springer, 255–278, 1996.
- Cai, Z. and Peng, C.: A study on training fine-tuning of convolutional neural networks, in: *2021 13th International Conference on Knowledge and Smart Technology (KST)*, 84–89, 2021.
- 625 Chagas, V. B. P., L. B. Chaffe, P., Addor, N., M. Fan, F., S. Fleischmann, A., C. D. Paiva, R., and Siqueira, V. A.: CAMELS-BR: Hydrometeorological time series and landscape attributes for 897 catchments in Brazil, *Earth Syst. Sci. Data*, 12, 2075–2096, <https://doi.org/10.5194/essd-12-2075-2020>, 2020.
- Cheng, M., Fang, F., Kinouchi, T., Navon, I. M., and Pain, C. C.: Long lead-time daily and monthly streamflow forecasting using machine learning methods, *J. Hydrol.*, 590, 125376, <https://doi.org/10.1016/j.jhydrol.2020.125376>, 2020.
- 630 Cho, K. and Kim, Y.: Improving streamflow prediction in the WRF-Hydro model with LSTM networks, *J. Hydrol.*, 605, 127297, <https://doi.org/10.1016/j.jhydrol.2021.127297>, 2022.
- Coxon, G., Addor, N., Bloomfield, J. P., Freer, J., Fry, M., Hannaford, J., Howden, N. J. K., Lane, R., Lewis, M., Robinson, E. L., Wagener, T., and Woods, R.: CAMELS-GB: hydrometeorological time series and landscape attributes for 671



- 635 catchments in Great Britain, *Earth Syst. Sci. Data*, 12, 2459–2483, <https://doi.org/10.5194/essd-12-2459-2020>, 2020.
- Curceac, S., Atkinson, P. M., Milne, A., Wu, L., and Harris, P.: Adjusting for Conditional Bias in Process Model Simulations of Hydrological Extremes: An Experiment Using the North Wyke Farm Platform, *Front. Artif. Intell.*, 3, 1–16, <https://doi.org/10.3389/frai.2020.565859>, 2020.
- Danapour, M., Højberg, A. L., Jensen, K. H., and Stisen, S.: Assessment of regional inter-basin groundwater flow using both  
640 simple and highly parameterized optimization schemes, *Hydrogeol. J.*, 27, 1929–1947, <https://doi.org/10.1007/s10040-019-01984-3>, 2019.
- Dembélé, M., Hrachowitz, M., Savenije, H. H. G., Mariéthoz, G., and Schaeffli, B.: Improving the Predictive Skill of a Distributed Hydrological Model by Calibration on Spatial Patterns With Multiple Satellite Data Sets, *Water Resour. Res.*, 56, 1–26, <https://doi.org/10.1029/2019WR026085>, 2020.
- 645 Devia, G. K., Ganasri, B. P., and Dwarakish, G. S.: A Review on Hydrological Models, *Aquat. Procedia*, 4, 1001–1007, <https://doi.org/10.1016/j.aqpro.2015.02.126>, 2015.
- Devitt, L., Neal, J., Coxon, G., Savage, J., and Wagener, T.: Flood hazard potential reveals global floodplain settlement patterns, *Nat. Commun.*, 14, 2801, <https://doi.org/10.1038/s41467-023-38297-9>, 2023.
- DHI: MIKE SHE User Guide and Reference Manual, 2020.
- 650 Duque, C., Nilsson, B., and Engesgaard, P.: Groundwater–surface water interaction in Denmark, *Wiley Interdiscip. Rev. Water*, 1–23, <https://doi.org/10.1002/wat2.1664>, 2023.
- Faticchi, S., Vivoni, E. R., Ogden, F. L., Ivanov, V. Y., Mirus, B., Gochis, D., Downer, C. W., Camporese, M., Davison, J. H., and Ebel, B.: An overview of current applications, challenges, and future trends in distributed process-based models in hydrology, *J. Hydrol.*, 537, 45–60, 2016.
- 655 Feng, D., Fang, K., and Shen, C.: Enhancing Streamflow Forecast and Extracting Insights Using Long-Short Term Memory Networks With Data Integration at Continental Scales, *Water Resour. Res.*, 56, 1–24, <https://doi.org/10.1029/2019WR026793>, 2020.
- Feng, D., Liu, J., Lawson, K., and Shen, C.: Differentiable, Learnable, Regionalized Process-Based Models With Multiphysical Outputs can Approach State-Of-The-Art Hydrologic Prediction Accuracy, *Water Resour. Res.*, 58, null,   
660 <https://doi.org/10.1029/2022WR032404>, 2022.
- Fowler, K. J. A., Acharya, S. C., Addor, N., Chou, C., and Peel, M. C.: CAMELS-AUS: Hydrometeorological time series and landscape attributes for 222 catchments in Australia, *Earth Syst. Sci. Data*, 13, 3847–3867, <https://doi.org/10.5194/essd-13-3847-2021>, 2021.
- Frame, J., Kratzert, F., Klotz, D., Gauch, M., Shelev, G., Gilon, O., Qualls, L. M., Gupta, H., and Nearing, G.: Deep learning rainfall-runoff predictions of extreme events, *Hydrol. Earth Syst. Sci.*, null, null, <https://doi.org/10.5194/hess-2021-423>, 2021a.
- Frame, J., Kratzert, F., Raney, A., Rahman, M., Salas, F., and Nearing, G.: Post-Processing the National Water Model with Long Short-Term Memory Networks for Streamflow Predictions and Model Diagnostics, *JAWRA J. Am. Water Resour. Assoc.*, 57, 885–905, <https://doi.org/10.1111/1752-1688.12964>, 2021b.



- 670 Frame, J. M., Kratzert, F., Raney, A., Rahman, M., Salas, F. R., and Nearing, G. S.: Post-Processing the National Water Model  
with Long Short-Term Memory Networks for Streamflow Predictions and Model Diagnostics, *J. Am. Water Resour. Assoc.*,  
57, 885–905, <https://doi.org/10.1111/1752-1688.12964>, 2021c.
- Fuente, L. A. De, Ehsani, M. R., Gupta, H. V., and Condon, L. E.: Towards Interpretable LSTM-based Modelling of  
Hydrological Systems, 1–29, 2023.
- Gers, F. A., Schmidhuber, J., and Cummins, F.: Learning to forget: Continual prediction with LSTM, *Neural Comput.*, 12,  
675 2451–2471, 2000.
- Ghorbani, A. and Zou, J.: Data shapley: Equitable valuation of data for machine learning, 36th Int. Conf. Mach. Learn. ICML  
2019, 2019-June, 4053–4065, 2019.
- Goldstein, A., Kapelner, A., Bleich, J., and Pitkin, E.: Peeking Inside the Black Box: Visualizing Statistical Learning With  
Plots of Individual Conditional Expectation, *J. Comput. Graph. Stat.*, 24, 44–65,  
680 <https://doi.org/10.1080/10618600.2014.907095>, 2015.
- Greff, K., Srivastava, R. K., Koutnik, J., Steunebrink, B. R., and Schmidhuber, J.: LSTM: A Search Space Odyssey, *IEEE  
Trans. Neural Networks Learn. Syst.*, 28, 2222–2232, <https://doi.org/10.1109/TNNLS.2016.2582924>, 2017.
- Gupta, H. V. and Kling, H.: On typical range, sensitivity, and normalization of Mean Squared Error and Nash-Sutcliffe  
Efficiency type metrics, *Water Resour. Res.*, 47, 2–4, <https://doi.org/10.1029/2011WR010962>, 2011.
- 685 Gupta, H. V., Kling, H., Yilmaz, K. K., and Martinez, G. F.: Decomposition of the mean squared error and NSE performance  
criteria: Implications for improving hydrological modelling, *J. Hydrol.*, 377, 80–91, 2009.
- Harrigan, S., Zsoter, E., Cloke, H., Salamon, P., and Prudhomme, C.: Daily ensemble river discharge reforecasts and real-time  
forecasts from the operational Global Flood Awareness System, *Hydrol. Earth Syst. Sci.*, 27, 1–19,  
<https://doi.org/10.5194/hess-27-1-2023>, 2023.
- 690 Hashemi, R., Brigode, P., Garambois, P. A., and Javelle, P.: How can we benefit from regime information to make more  
effective use of long short-term memory (LSTM) runoff models?, *Hydrol. Earth Syst. Sci.*, 26, 5793–5816,  
<https://doi.org/10.5194/hess-26-5793-2022>, 2022.
- Hauswirth, S. M., Bierkens, M. F. P., Beijk, V., and Wanders, N.: The potential of data driven approaches for quantifying  
hydrological extremes, *Adv. Water Resour.*, 155, 104017, <https://doi.org/10.1016/j.advwatres.2021.104017>, 2021.
- 695 Henriksen, H. J., Troldborg, L., Nyegaard, P., Sonnenborg, T. O., Refsgaard, J. C., and Madsen, B.: Methodology for  
construction, calibration and validation of a national hydrological model for Denmark, *J. Hydrol.*, 280, 52–71,  
[https://doi.org/https://doi.org/10.1016/S0022-1694\(03\)00186-0](https://doi.org/https://doi.org/10.1016/S0022-1694(03)00186-0), 2003.
- Henriksen, H. J., Kragh, S. J., Gotfredsen, J., Ondracek, M., van Til, M., Jakobsen, A., Schneider, R. J. M., Koch, J., Troldborg,  
L., Rasmussen, P., Pasten-Zapata, E., and Stisen, S.: Udvikling af landsdækkende modelberegninger af terrænnære  
700 hydrologiske forhold i 100m grid ved anvendelse af DK-modellen: Dokumentationsrapport vedr. modelleverancer til  
Hydrologisk Informations- og Prognosesystem. Udarbejdet som en del af Den Fællesoffen, GEUS,  
<https://doi.org/10.22008/gpub/38113>, 2021.



- Henriksen, H. J., Schneider, R., Koch, J., Ondracek, M., Troldborg, L., Seidenfaden, I. K., Kragh, S. J., Bøgh, E., and Stisen, S.: A New Digital Twin for Climate Change Adaptation, Water Management, and Disaster Risk Reduction (HIP Digital Twin), *Water (Switzerland)*, 15, <https://doi.org/10.3390/w15010025>, 2023.
- Herrera, P. A., Marazuela, M. A., and Hofmann, T.: Parameter estimation and uncertainty analysis in hydrological modeling, *Wiley Interdiscip. Rev. Water*, 9, 1–23, <https://doi.org/10.1002/wat2.1569>, 2022.
- Hochreiter, S. and Schmidhuber, J.: Long Short-Term Memory, *Neural Comput.*, 9, 1735–1780, <https://doi.org/10.1162/neco.1997.9.8.1735>, 1997.
- Höge, M., Kauzlaric, M., Siber, R., Schönenberger, U., Horton, P., Schwanbeck, J., Floriancic, M. G., Viviroli, D., Wilhelm, S., Sikorska-Senoner, A. E., Addor, N., Brunner, M., Pool, S., Zappa, M., and Fenicia, F.: CAMELS-CH: hydro-meteorological time series and landscape attributes for 331 catchments in hydrologic Switzerland, *Earth Syst. Sci. Data Discuss.*, 2023.
- Højberg, A. L., Troldborg, L., Nyegaard, P., Ondracek, M., Stisen, S., S. Stisen, and Stisen, S.: Handling and linking data and hydrological models – experiences from the Danish national water resources model (DK-model), *Modelcare2010*, 141–144, 2009.
- Højberg, A. L., Troldborg, L., Stisen, S., Christensen, B. B. S. S., and Henriksen, H. J.: Stakeholder driven update and improvement of a national water resources model, *Environ. Model. Softw.*, 40, 202–213, <https://doi.org/10.1016/j.envsoft.2012.09.010>, 2013.
- Hoy, A. Q.: Protecting water resources calls for international efforts, *Science (80-. )*, 356, 814–815, <https://doi.org/10.1126/science.356.6340.814>, 2017.
- Hunt, K. M. R., Matthews, G. R., Pappenberger, F., and Prudhomme, C.: Using a long short-term memory (LSTM) neural network to boost river streamflow forecasts over the western United States, *Hydrol. Earth Syst. Sci.*, 26, 5449–5472, <https://doi.org/10.5194/hess-26-5449-2022>, 2022.
- Käding, C., Rodner, E., Freytag, A., and Denzler, J.: Fine-tuning deep neural networks in continuous learning scenarios, *Lect. Notes Comput. Sci. (including Subser. Lect. Notes Artif. Intell. Lect. Notes Bioinformatics)*, 10118 LNCS, 588–605, [https://doi.org/10.1007/978-3-319-54526-4\\_43](https://doi.org/10.1007/978-3-319-54526-4_43), 2017.
- Kawaguchi, K., Bengio, Y., and Kaelbling, L.: Generalization in Deep Learning, *Math. Asp. Deep Learn.*, 112–148, <https://doi.org/10.1017/9781009025096.003>, 2022.
- Ke, G., Meng, Q., Finley, T., Wang, T., Chen, W., Ma, W., Ye, Q., and Liu, T. Y.: LightGBM: A highly efficient gradient boosting decision tree, *Adv. Neural Inf. Process. Syst.*, 2017-Decem, 3147–3155, 2017.
- Klotz, D., Kratzert, F., Gauch, M., Keefe Sampson, A., Brandstetter, J., Klambauer, G., Hochreiter, S., and Nearing, G.: Uncertainty estimation with deep learning for rainfall-runoff modeling, *Hydrol. Earth Syst. Sci.*, 26, 1673–1693, <https://doi.org/10.5194/hess-26-1673-2022>, 2022.
- Koch, J. and Schneider, R.: Long short-term memory networks enhance rainfall-runoff modelling at the national scale of Denmark, *GEUS Bull.*, 49, 1–7, <https://doi.org/10.34194/geusb.v49.8292>, 2022.
- Koch, J., Cornelissen, T., Fang, Z., Bogena, H., Diekkrüger, B., Kollet, S., and Stisen, S.: Inter-comparison of three distributed



- hydrological models with respect to seasonal variability of soil moisture patterns at a small forested catchment, *J. Hydrol.*, 533, 234–249, 2016.
- 740 Koch, J., Gotfredsen, J., Schneider, R., Troldborg, L., Stisen, S., and Henriksen, H. J.: High Resolution Water Table Modeling of the Shallow Groundwater Using a Knowledge-Guided Gradient Boosting Decision Tree Model, *Front. Water*, 3, 1–14, <https://doi.org/10.3389/frwa.2021.701726>, 2021.
- Konapala, G., Kao, S. C., Painter, S. L., and Lu, D.: Machine learning assisted hybrid models can improve streamflow simulation in diverse catchments across the conterminous US, *Environ. Res. Lett.*, 15, <https://doi.org/10.1088/1748-9326/aba927>, 2020.
- 745 Kratzert, F., Klotz, D., Brenner, C., Schulz, K., and Herrnegger, M.: Rainfall-runoff modelling using Long Short-Term Memory (LSTM) networks, *Hydrol. Earth Syst. Sci.*, 22, 6005–6022, <https://doi.org/10.5194/hess-22-6005-2018>, 2018.
- Kratzert, F., Herrnegger, M., Klotz, D., Hochreiter, S., and Klambauer, G.: NeuralHydrology – Interpreting LSTMs in Hydrology, *Lect. Notes Comput. Sci. (including Subser. Lect. Notes Artif. Intell. Lect. Notes Bioinformatics)*, 11700 LNCS, 347–362, [https://doi.org/10.1007/978-3-030-28954-6\\_19](https://doi.org/10.1007/978-3-030-28954-6_19), 2019a.
- 750 Kratzert, F., Klotz, D., Herrnegger, M., Sampson, A. K., Hochreiter, S., and Nearing, G. S.: Toward Improved Predictions in Ungauged Basins: Exploiting the Power of Machine Learning, *Water Resour. Res.*, 55, 11344–11354, <https://doi.org/10.1029/2019WR026065>, 2019b.
- Kratzert, F., Klotz, D., Hochreiter, S., and Nearing, G. S.: A note on leveraging synergy in multiple meteorological data sets with deep learning for rainfall-runoff modeling, *Hydrol. Earth Syst. Sci.*, 25, 2685–2703, <https://doi.org/10.5194/hess-25-2685-2021>, 2021.
- 755 Kratzert, F., Gauch, M., Nearing, G., and Klotz, D.: NeuralHydrology — A Python library for Deep Learning research in hydrology, *J. Open Source Softw.*, 7, 4050, <https://doi.org/10.21105/joss.04050>, 2022.
- Kumari, N., Srivastava, A., Sahoo, B., Raghuvanshi, N. S., and Bretreger, D.: Identification of Suitable Hydrological Models for Streamflow Assessment in the Kangsabati River Basin, India, by Using Different Model Selection Scores, *Nat. Resour. Res.*, 30, 4187–4205, <https://doi.org/10.1007/s11053-021-09919-0>, 2021.
- 760 Lees, T., Buechel, M., Anderson, B., Slater, L., Reece, S., Coxon, G., and Dadson, S.: Benchmarking data-driven rainfall-runoff models in Great Britain: a comparison of long short-term memory (LSTM)-based models with four lumped conceptual models, *Hydrol. Earth Syst. Sci.*, null, null, <https://doi.org/10.5194/hess-25-5517-2021>, 2021.
- Li, D. and Zhang, H. R.: Improved Regularization and Robustness for Fine-tuning in Neural Networks, *Adv. Neural Inf. Process. Syst.*, 33, 27249–27262, 2021.
- 765 Liu, S., Wang, J., Wang, H., and Wu, Y.: Post-processing of hydrological model simulations using the convolutional neural network and support vector regression, *Hydrol. Res.*, 53, 605–621, <https://doi.org/10.2166/nh.2022.004>, 2022.
- MacNeil, D. and Eliasmith, C.: Fine-tuning and the stability of recurrent neural networks, *PLoS One*, 6, <https://doi.org/10.1371/journal.pone.0022885>, 2011.
- 770 Moges, E., Demissie, Y., Larsen, L., and Yassin, F.: Review: Sources of hydrological model uncertainties and advances in



- their analysis, *Water (Switzerland)*, 13, 1–23, <https://doi.org/10.3390/w13010028>, 2021.
- Nash, J. E. and Sutcliffe, J. V.: River flow forecasting through conceptual models part I—A discussion of principles, *J. Hydrol.*, 10, 282–290, 1970.
- Nearing, G. S., Klotz, D., Frame, J. M., Gauch, M., Gilon, O., Kratzert, F., Sampson, A. K., Shalev, G., and Nevo, S.: Technical  
775 note: Data assimilation and autoregression for using near-real-time streamflow observations in long short-term memory  
networks, *Hydrol. Earth Syst. Sci.*, 26, 5493–5513, <https://doi.org/10.5194/hess-26-5493-2022>, 2022.
- Nevo, S., Morin, E., Gerzi Rosenthal, A., Metzger, A., Barshai, C., Weitzner, D., Voloshin, D., Kratzert, F., Elidan, G., Dror,  
G., Begelman, G., Nearing, G., Shalev, G., Noga, H., Shavitt, I., Yuklea, L., Royz, M., Giladi, N., Peled Levi, N., Reich, O.,  
Gilon, O., Maor, R., Timnat, S., Shechter, T., Anisimov, V., Gigi, Y., Levin, Y., Moshe, Z., Ben-Haim, Z., Hassidim, A., and  
780 Matias, Y.: Flood forecasting with machine learning models in an operational framework, *Hydrol. Earth Syst. Sci.*, 26, 4013–  
4032, <https://doi.org/10.5194/hess-26-4013-2022>, 2022.
- Pakoksung, K. and Takagi, M.: Effect of DEM sources on distributed hydrological model to results of runoff and inundation  
area, *Model. Earth Syst. Environ.*, 7, 1891–1905, <https://doi.org/10.1007/s40808-020-00914-7>, 2021.
- Paszke, A., Gross, S., Massa, F., Lerer, A., Bradbury, J., Chanan, G., Killeen, T., Lin, Z., Gimelshein, N., Antiga, L.,  
785 Desmaison, A., Köpf, A., Yang, E., DeVito, Z., Raison, M., Tejani, A., Chilamkurthy, S., Steiner, B., Fang, L., Bai, J., and  
Chintala, S.: PyTorch: An imperative style, high-performance deep learning library, *Adv. Neural Inf. Process. Syst.*, 32, 2019.
- Rahmani, F., Lawson, K., Ouyang, W., Appling, A., Oliver, S., and Shen, C.: Exploring the exceptional performance of a deep  
learning stream temperature model and the value of streamflow data, *Environ. Res. Lett.*, 16, null,  
<https://doi.org/10.1088/1748-9326/abd501>, 2020.
- 790 Rätsch, G.: A brief introduction into machine learning, *21st Chaos Commun. Congr.*, 1–6, 2004.
- Refsgaard, J. C., Stisen, S., and Koch, J.: Hydrological process knowledge in catchment modelling – Lessons and perspectives  
from 60 years development, *Hydrol. Process.*, 36, 1–20, <https://doi.org/10.1002/hyp.14463>, 2022.
- Roy, A., Kasiviswanathan, K. S., Patidar, S., Adeloye, A. J., Soundharajan, B. S., and Ojha, C. S. P.: A Novel Physics-Aware  
Machine Learning-Based Dynamic Error Correction Model for Improving Streamflow Forecast Accuracy, *Water Resour. Res.*,  
795 59, <https://doi.org/10.1029/2022WR033318>, 2023.
- Sahraei, S., Asadzadeh, M., and Unduche, F.: Signature-based multi-modelling and multi-objective calibration of hydrologic  
models: Application in flood forecasting for Canadian Prairies, *J. Hydrol.*, 588, 125095, 2020.
- Satoh, Y., Yoshimura, K., Pokhrel, Y., Kim, H., Shiogama, H., Yokohata, T., Hanasaki, N., Wada, Y., Burek, P., Byers, E.,  
Schmied, H. M., Gerten, D., Ostberg, S., Gosling, S. N., Boulange, J. E. S., and Oki, T.: The timing of unprecedented  
800 hydrological drought under climate change, *Nat. Commun.*, 13, <https://doi.org/10.1038/s41467-022-30729-2>, 2022.
- Scharling, M.: Klimagrid Danmark - Nedbør, lufttemperatur og potentiel fordampning 20X20 & 40x40 km -  
Metodebeskrivelse, Danish Meteorol. Inst., 1999a.
- Scharling, M.: Klimagrid Danmark Nedbør 10x10 km (ver. 2) - Metodebeskrivelse, Danish Meteorol. Inst., 15–17, 1999b.
- Schneider, R., Henriksen, H. J., and Stisen, S.: A robust objective function for calibration of groundwater models in light of





- 805 deficiencies of model structure and observations, *J. Hydrol.*, 613, 128339, <https://doi.org/10.1016/j.jhydrol.2022.128339>, 2022a.
- Schneider, R., Koch, J., Troldborg, L., Henriksen, H. J., and Stisen, S.: Machine-learning-based downscaling of modelled climate change impacts on groundwater table depth, *Hydrol. Earth Syst. Sci.*, 26, 5859–5877, <https://doi.org/10.5194/hess-26-5859-2022>, 2022b.
- 810 Shen, Y., Ruijsch, J., Lu, M., Sutanudjaja, E. H., and Karssenber, D.: Random forests-based error-correction of streamflow from a large-scale hydrological model: Using model state variables to estimate error terms, *Comput. Geosci.*, 159, 105019, <https://doi.org/10.1016/j.cageo.2021.105019>, 2022.
- Silvestro, F., Gabellani, S., Rudari, R., Delogu, F., Laiolo, P., and Boni, G.: Uncertainty reduction and parameter estimation of a distributed hydrological model with ground and remote-sensing data, *Hydrol. Earth Syst. Sci.*, 19, 1727–1751, <https://doi.org/10.5194/hess-19-1727-2015>, 2015.
- 815 Slater, L. J., Arnal, L., Boucher, M. A., Chang, A. Y. Y., Moulds, S., Murphy, C., Nearing, G., Shalev, G., Shen, C., Speight, L., Villarini, G., Wilby, R. L., Wood, A., and Zappa, M.: Hybrid forecasting: blending climate predictions with AI models, *Hydrol. Earth Syst. Sci.*, null, null, <https://doi.org/10.5194/hess-27-1865-2023>, 2023.
- Soltani, M., Bjerre, E., Koch, J., and Stisen, S.: Integrating remote sensing data in optimization of a national water resources model to improve the spatial pattern performance of evapotranspiration, *J. Hydrol.*, 603, 127026, <https://doi.org/10.1016/j.jhydrol.2021.127026>, 2021.
- 820 Stisen, S., Sonnenborg, T. O., Højberg, A. L., Troldborg, L., and Refsgaard, J. C.: Evaluation of Climate Input Biases and Water Balance Issues Using a Coupled Surface-Subsurface Model, *Vadose Zo. J.*, 10, 37–53, <https://doi.org/10.2136/vzj2010.0001>, 2011.
- 825 Stisen, S., Ondracek, M., Troldborg, L., Schneider, R. J. M., and Til, M. J. van: National Vandressource Model. Modelopstilling og kalibrering af DK-model 2019, GEUS, Copenhagen, <https://doi.org/10.22008/gpub/32631>, 2020.
- Sutskever, I., Vinyals, O., and Le, Q. V.: Sequence to sequence learning with neural networks, *Adv. Neural Inf. Process. Syst.*, 4, 3104–3112, 2014.
- Tan, C., Sun, F., Kong, T., Zhang, W., Yang, C., and Liu, C.: A survey on deep transfer learning, *Lect. Notes Comput. Sci.* (including Subser. Lect. Notes Artif. Intell. Lect. Notes Bioinformatics), 11141 LNCS, 270–279, [https://doi.org/10.1007/978-3-030-01424-7\\_27](https://doi.org/10.1007/978-3-030-01424-7_27), 2018.
- 830 Tang, S., Sun, F., Liu, W., Wang, H., Feng, Y., and Li, Z.: Optimal Postprocessing Strategies With LSTM for Global Streamflow Prediction in Ungauged Basins, *Water Resour. Res.*, 59, 1–16, <https://doi.org/10.1029/2022WR034352>, 2023.
- Wang, Y., Liu, J., Li, C., Liu, Y., Xu, L., and Yu, F.: A data-driven approach for flood prediction using grid-based meteorological data, *Hydrol. Process.*, 37, <https://doi.org/10.1002/hyp.14837>, 2023.
- 835 Wang, Y. H., Gupta, H. V., Zeng, X., and Niu, G. Y.: Exploring the Potential of Long Short-Term Memory Networks for Improving Understanding of Continental- and Regional-Scale Snowpack Dynamics, *Water Resour. Res.*, 58, <https://doi.org/10.1029/2021WR031033>, 2022.



- 840 Wi, S. and Steinschneider, S.: On the need for physical constraints in deep learning rainfall-runoff projections under climate change, 1–46, 2023.
- Wilbrand, K., Taormina, R., ten Veldhuis, M., Visser, M., Hrachowitz, M., Nuttall, J., and Dahm, R.: Predicting streamflow with LSTM networks using global datasets, <https://doi.org/10.3389/frwa.2023.1166124>, 2023.
- Wu, H., Hu, T., Liu, Y., Zhou, H., Wang, J., and Long, M.: TimesNet: Temporal 2D-Variation Modeling for General Time Series Analysis, 1–23, 2022.
- 845 Yan, J. and Smith, K. R.: SIMULATION OF INTEGRATED SURFACE WATER AND GROUND WATER SYSTEMS-MODEL FORMULATION 1, JAWRA J. Am. Water Resour. Assoc., 30, 879–890, 1994.
- Yilmaz, K. K., Gupta, H. V., and Wagener, T.: A process-based diagnostic approach to model evaluation: Application to the NWS distributed hydrologic model, *Water Resour. Res.*, 44, 1–18, <https://doi.org/10.1029/2007WR006716>, 2008.
- 850 Zhang, T., Liang, Z., Li, W., Wang, J., Hu, Y., and Li, B.: Statistical post-processing of precipitation forecasts using circulation classifications and spatiotemporal deep neural networks, *Hydrol. Earth Syst. Sci. Discuss.*, 1–26, 2023.
- Zhang, Y., Ragetti, S., Molnar, P., Fink, O., and Peleg, N.: Generalization of an Encoder-Decoder LSTM model for flood prediction in ungauged catchments, *J. Hydrol.*, null, null, <https://doi.org/10.1016/j.jhydrol.2022.128577>, 2022.